POLITECNICO DI TORINO
Repository ISTITUZIONALE

Porous Zinc Oxide Thin Films: Synthesis Approaches and Applications

Original
Porous Zinc Oxide Thin Films: Synthesis Approaches and Applications / Laurenti, M., Cauda, V.A.. - In: COATINGS. - ISSN 2079-6412. - ELETTRONICO. - 8:2(2018), p. 67. [10.3390/coatings8020067]

Availability:
This version is available at: 11583/2700182 since: 2020-06-18T10:23:16Z

Publisher:
MDPI

Published
DOI:10.3390/coatings8020067

Terms of use:

This article is made available under terms and conditions as specified in the corresponding bibliographic description in the repository

Publisher copyright

(Article begins on next page)

22 June 2026

coatings

MDPI

Review

Porous Zinc Oxide Thin Films: Synthesis Approaches and Applications

Marco Laurenti * and Valentina Cauda

Department of Applied Science and Technology, Politecnico di Torino, C.so Duca degli Abruzzi 24, 10129 Turin, Italy; valentina.cauda@polito.it

* Correspondence: marco.laurenti@polito.it; Tel.: +39-011-090-7394

Received: 17 December 2017; Accepted: 7 February 2018; Published: 9 February 2018

Abstract: Zinc oxide (ZnO) thin films have been widely investigated due to their multifunctional properties, i.e., catalytic, semiconducting and optical. They have found practical use in a wide number of application fields. However, the presence of a compact micro/nanostructure has often limited the resulting material properties. Moreover, with the advent of low-dimensional ZnO nanostructures featuring unique physical and chemical properties, the interest in studying ZnO thin films diminished more and more. Therefore, the possibility to combine at the same time the advantages of thin-film based synthesis technologies together with a high surface area and a porous structure might represent a powerful solution to prepare ZnO thin films with unprecedented physical and chemical characteristics that may find use in novel application fields. Within this scope, this review offers an overview on the most successful synthesis methods that are able to produce ZnO thin films with both framework and textural porosities. Moreover, we discuss the related applications, mainly focused on photocatalytic degradation of dyes, gas sensor fabrication and photoanodes for dye-sensitized solar cells.

Keywords: zinc oxide; thin films; high surface area; porous structure; sputtering; electrodeposition; spray pyrolysis; template-assisted methods

1. Introduction

Zinc Oxide (ZnO) is a well-known metal oxide material showing interesting biocompatible [1,2], semiconducting [3], optical [4], photocatalytic [5], resistive switching [6] and piezoelectric properties [7]. Among the main advantages, the easy preparation of ZnO in the form of thin films [8], nanowires [9], nanorods [10], crystalline nanoparticles [11] and flower-like structures [12] has strongly encouraged its investigation for various applications, including ultraviolet (UV) photodetectors [13], photoanodes [14], photocatalysis [5], gas sensors [15] and energy harvesting systems [16]. Historically speaking, ZnO thin films prepared by means of several synthetic approaches have been first investigated, and the resulting properties exploited for a huge number of application fields [17]. These include surface acoustic wave sensors [18], thin-film based transistors [19] and gas sensors [20]. However, ZnO thin-film based technologies suffer from some major limitations, mainly due to their intrinsic low surface area combined with the lack of a framework porosity, i.e., porosity contained within each particle composing the framework [21]. Actually, these aspects are of particular importance especially for bio- and gas-sensing applications; low surface areas prevent effective surface chemical modification treatments, limiting the sensing response and selective properties. On the other side, the absence of framework porosities prevents the possibility to host molecules of interest such as drugs and proteins, thereby limiting the use of ZnO thin films in biomedical applications like drug-delivery systems and tissue engineering. Some alternative solutions have been explored in view of improving at least the surface area. To this purpose, plasma-assisted chemical vapor deposition (CVD) approaches represented a valid solution for preparing low-density structure ZnO thin films [22].

Actually, plasma-CVD allowed the catalyst-free growth of ZnO nanocolumnar thin films with a more pronounced textural porosity, i.e., porosity due to voids and spaces formed by contacts among nanocolumns. However, no framework porosity, i.e., pores within the single ZnO nanocolumn, was achieved. Anyway, thanks to the higher surface area, the proposed ZnO nanocolumnar films were successfully applied to gas sensing [23], solar cells [24] and photocatalysis [25].

Most of the limitations mentioned above have been successfully overcome with the advent of low-dimensional ZnO structures. A wide plethora of synthesis methods have been explored and optimized, allowing to obtain ZnO structures with various shapes and morphologies, ranging from the micrometer to the nanometer scale. Among them, ZnO hollow-sphere particles and quantum dots are the most promising ones [26–28]. With a high surface area combined to a framework porosity, such low-dimensional ZnO structures exhibited improved physical properties, thanks to the presence of physical quantum confinement effects occurring in low-dimensional nanomaterials [29–31]. Despite the promising behaviors, some major concerns still prevent the integration of low-dimensional ZnO nanomaterials into final product applications, such as limitations in the scalability of the synthetic approaches towards large areas, as well as the reproducibility of the resulting materials properties. Therefore, the thin-film based technology still represents one of the most valid solutions in terms of industrial scalability and integration of functional materials into product applications.

Within this scope, this review aims at presenting an overview on the synthesis and applications of porous ZnO thin-film with well-defined textural and framework porosities. The most successful methods are found to be physical vapor depositions, especially concerning pulsed laser deposition and sputtering techniques, electrodeposition and spray pyrolysis. Other wet-chemistry approaches and template-assisted growth methods are discussed as well. In the next paragraphs, the main achievements in terms of various porous ZnO morphologies and corresponding application properties are discussed and correlated to each specific synthetic approach.

2. Physical Vapor Deposition of Porous ZnO Thin Films

Physical Vapor Deposition (PVD) methods are based on the formation of a vapor phase from a solid source material, and the following condensation on a substrate surface. Atoms and/or molecules making the vapor phase are physically extracted from the source material. This extraction process can be pursued by using various sources of energy, each one characteristic of the particular deposition method. For example, the presence of plasma is required for sputtering process, while high-energy photons coming from a laser source are exploited in the case of pulsed laser deposition (PLD). The formation process of thin films may be roughly summarized into the adsorption, nucleation and coalescence steps. The first one deals with the adsorption of atoms and/or molecules, coming from the vapor phase, on a substrate surface (adatoms). This process is driven by physisorption, i.e., weak electrostatic interactions due to Van der Waals forces, and/or chemisorption, i.e., formation of strong chemical bonds between atoms and the surface. After adsorption, nucleation and coalescence steps take place. In such situations, different adatoms start to aggregate together (nucleation), resulting in the formation of islands. These can further increase in dimensions and coalesce together, finally leading to the formation of a continuous thin film network that cover the whole substrate surface, if desired. Depending on the specific deposition parameters, each of the abovementioned steps can be properly influenced to promote the growth of island separately, avoiding the formation of a compact film. The final result would in this case lead to thin porous film, with specific micro/nanostructures and morphologies.

The following paragraphs aim at presenting an overview of the main results achieved for the growth of high surface areas and porous ZnO thin films by PVD methods, with a particular focus on the use of sputtering and PLD techniques.

2.1. Sputtering

Sputtering is a plasma-assisted PVD process where collisions between high-energy ions and the source material (target) are exploited for the formation of a vapor phase. Plasma is obtained by

injecting a noble gas (usually argon) into the deposition chamber which is ionized by the application of a proper direct-current (DC)/radio-frequency (RF) signal voltage between a cathode, where the target is clamped, and the rest of the chamber. The impinging of ions on the target surface allows the extraction of atoms. Once the vapor phase is formed, condensation on the substrate surface takes place and thin-film formation may be pursued by the following nucleation and coalescence steps. Sputtering technology has been widely investigated because of its multiple advantages, as it is a high-yield production technology, compatible with integrated-circuit processing, and allows for the homogeneous deposition of materials on wide-area substrates. Moreover, sputtering does not necessarily require the use of high deposition temperatures. Therefore, it is compatible with the use of a wide range of substrates, including polymers.

The possibility to obtain a uniform distribution of nanopores in sputtered ZnO thin films was exploited for the fabrication of bio-electrodes for cholesterol detection [32]. ZnO thin films were grown on gold-coated glass substrates by RF magnetron sputtering, using a very high deposition pressure (50 mTorr). This allowed to introduce a uniform distribution of nanopores within the thin film network, as confirmed by Atomic Force Microscope (AFM) analyses. The formation of this particular structure (average rms roughness ~4 nm) and of the nanopores was mainly due to the high sputtering pressure used for the growth of ZnO thin film, since inducing a strong in-situ bombardment of the growing thin film from high-energy species. The resulting high-surface area was successfully exploited to immobilize Cholesterol Oxidase (ChO_x) enzyme onto the nanoporous ZnO thin-film/Au/glass bio-electrodes. Both cyclic voltammetry measurements and optical studies revealed a stable and linear response of the ChO_x/ZnO/Au bio-electrode up to 10 weeks, coupled with a promising sensitivity (detection of cholesterol concentration in the range 25–400 $mg \cdot dL^{-1}$).

Instead of using high pressure regimes during sputtering deposition, an alternative way to introduce a controlled porosity within the thin film structure is the use of a glancing-angle sputter deposition approach. By following a one-step oblique-angle deposition method, non-polar ZnO thin films showing a high crystal quality and porosity were successfully grown on glass substrates [33]. In this case, the sputtering gun was collimated at an oblique angle of 30° with respect to the substrate surface, without any substrate rotation. Figure 1 shows the particular surface morphology featured from ZnO thin films obtained with this method. These were composed by highly crystalline ZnO microrods (approximately 1–2 μm in length and 200–600 nm in width), mainly oriented along the [002] crystallographic direction, nearly parallel to the substrate surface. At the beginning of the deposition process, the ZnO microrods were densely packed to each other. Then, formation of pores was observed by increasing the film thickness. This approach favored the gradual rotation of the *c*-axis growth direction, from the vertical to the nearly lateral direction with respect to the substrate, finally leading to the formation of gaps between neighbor crystal grains, and hence to the formation of pores.

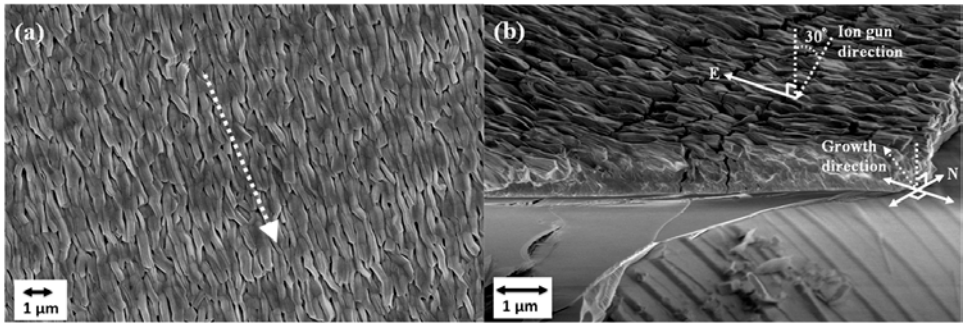

Figure 1. Scanning Electron Microscope low-magnification images: (**a**) Top view of as-synthesized ZnO film on glass substructure, where the white arrow indicates the projection of the incident flux on the film; (**b**) Cross-sectional view of the sample, where the ion flux and growth direction are denoted. Adapted with permission from [33]; Copyright 2013 Elsevier.

Alternatively, the introduction of a tunable, porous microstructure within ZnO thin films has been observed by using unbalanced magnetron sputtering conditions [34]. To prove the effect of the magnetron configuration, the porosity of ZnO thin films sputtered in three different types of magnetron electrode configurations was considered, and its effect on the resulting crystal structure and UV photo-response investigated. The unbalanced conditions were obtained by progressively lowering the strength of the central magnet in the magnetron, in order to increase the ion and electron flux at the substrate. Accordingly, the plasma confinement conditions could be changed. In the case of weak central magnet conditions, a very intense bombardment effect on the substrate occurred, with the erosion of the source material occurring mainly in the center. On the other hand, minimal bombardment effects were obtained in presence of a balanced magnetron configuration. X-ray Diffraction (XRD) analyses revealed the transition from a randomly oriented, polycrystalline ZnO thin film with no (002) orientation for the unbalanced configuration, to a strong *c*-axis orientation along the (002) direction for the balanced case. In comparison with high (002)-oriented dense columnar ZnO thin films, the presence of a mixed crystallographic orientation, promoted from the unbalanced magnetron conditions, favored films transparency, the formation of smaller grain size and the arise of a porous microstructure. The porous voids, coupled to the lower kinetic energy of species sputtered in unbalanced magnetron conditions, favored oxygen trapping within the thin film structure, especially at grain boundaries. Such trapped oxygen actively participated to photo-desorption and adsorption processes occurring during UV irradiation of the sample, thereby improving UV photoresponse (rise time of 792 ms and fall time of 805 ms under low radiation intensity of 9.5 $mW \cdot cm^2$ at λ_{UV} = 365 nm). In contrast, no appreciable UV photoresponse was observed for dense ZnO films.

Porous ZnO thin films were also obtained by thermally oxidizing metallic Zn films deposited by DC sputtering [35]. The effect of using different pressure conditions (2 and 10 mTorr) and deposition atmospheres (pure Ar instead of mixed Ar + O_2, 10%) was first investigated. Figure 2a shows the morphology of Zn films grown with an Ar pressure of 2 mTorr.

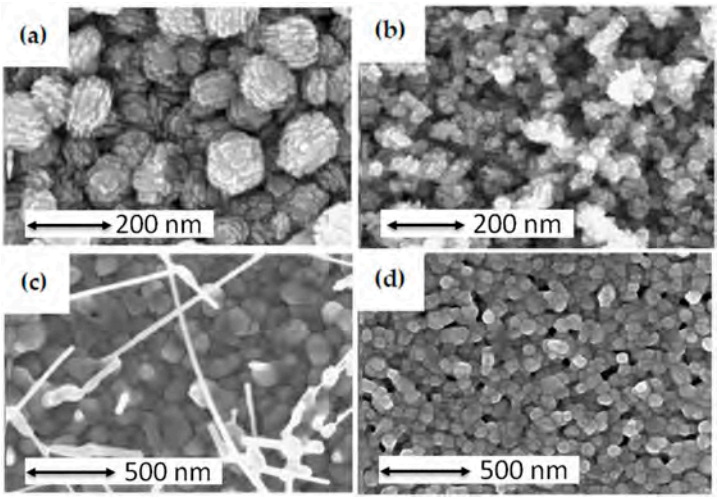

Figure 2. Surface morphologies of Zn films deposited on glass substrates with magnetron sputtering: (**a**) Ar, 2 mTorr; and (**b**) Ar + O_2, 2 mTorr. Surface morphology of ZnO films formed by thermal oxidation of Zn films at 600 °C in air for 1 h: (**c**) deposited in Ar, 10 mTorr; and (**d**) deposited in Ar + O_2, 10 mTorr. Adapted with permission from [35]; Copyright 2005 Elsevier.

The presence of hexahedron-like particles (average size of 200 nm) appearing as stacks of many flat facets, was noticed. By further increasing the pressure, the particle size slightly decreased and the outer flat facets broke. By including a small oxygen percentage to the deposition atmosphere, the arise of very fine particles (~20 nm) was observed, as shown in Figure 2b. These were interconnected together, forming a porous network. When the total pressure increased to 10 mTorr, the film showed many clusters

(~150 nm) made of fine particles (~50 nm). The metallic Zn films were further oxidized in air at 600 °C for 1 h to be totally converted into ZnO, as confirmed by XRD analyses. The morphologies of the resulting ZnO thin films were strongly correlated with the deposition conditions of the starting Zn films.

Figure 2c shows the surface morphology of ZnO films obtained starting from Zn layers grown in pure Ar conditions at 10 mTorr. Independently of the pressure value used during Zn deposition, a dense and compact structure was obtained after thermal oxidation, together with the presence of oxide whiskers on the surface. On the other side, the surface morphology changed after the oxidation of Zn films obtained from a mixed Ar + O_2 atmosphere. In this case, the Zn films grown at low pressure still showed a relatively dense structure, made of very fine particles (~40 nm) and tower-like clusters due to some particles aggregation. However, the films deposited at a higher pressure possessed a porous structure composed of particles in the range of 60–90 nm after oxidation, as clearly visible in Figure 2d. The observed morphological changes both for Zn and ZnO thin films and the presence of a porous structure were mainly discussed in terms of deposition atmosphere conditions. The incorporation of oxygen during sputtering resulted in the formation of two phases, Zn and ZnO, and into the promotion of fine particles, eventually showing a Zn/ZnO core-shell configuration. Such structures could promote the nucleation process of oxides in the initial oxidation stage, inhibit evaporation of molten components and limit preferential growth along specific directions, thus resulting in the formation of porous films with fine particles without whisker oxides. Finally, the optical properties of the samples were investigated and correlated to the corresponding morphologies. Dense ZnO films coming from Zn films deposited in pure Ar exhibited low optical transmittance in visible light region, extremely strong UV emission and weak defect-related photoluminescence (PL) emissions. On the other hand, the porous multiphase ZnO showed a high transparency and relatively strong defect-related PL emission at room temperature.

In a similar way, porous nanobranched ZnO thin films with average thicknesses ranging from few μm up to tens of μm, were easily fabricated by a two-step synthetic approach, involving RF magnetron sputtering of metallic Zn films and their oxidation by thermal annealing in ambient air a 380 °C for 2 h [36] or alternatively, by low-temperature water-vapor oxidation treatment [37]. The synthesis of metallic Zn films was performed at room temperature in a pure Ar atmosphere, using very mild conditions in terms of applied RF signal, Ar flow and pressure. In this way, a porous metallic network with a very high surface area was obtained still from the beginning of the synthesis process (Figure 3a), and was completely preserved after the oxidation treatments mentioned above (Figure 3b,c).

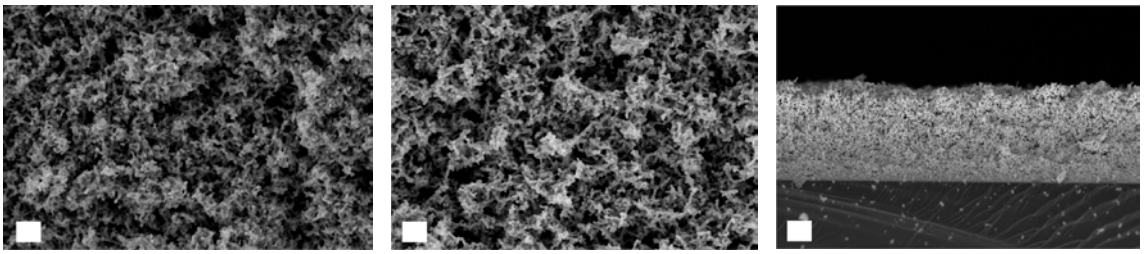

(**a**) (**b**) (**c**)

Figure 3. Field Emission Scanning Electron Microscope images of porous Zn thin films: (**a**) as-prepared; (**b**,**c**) after conversion into ZnO by thermal oxidation. Scale bar for (**a**) and (**b**) is 400 nm, for (**c**) is 2 μm.

The possibility to obtain the so-called "sponge-like" porous thin-film morphology was explained through a modified "structure zone" model [36]. According to this, specific thin-film morphologies are defined considering the ratio between the substrate temperature and the melting temperature of the deposited material. Therefore, totally different morphologies can be obtained by changing the substrate temperature. On the basis of the structure zone model, the substrate temperature should lie at around ~350 K so that the sponge-like morphology can be formed in the specific case of Zn thin films (melting temperature ~690 K). Such a local heating can be easily achieved during sputtering depositions and

without providing any intentional heating to the substrates. This is due to the energy exchange occurring when high-energy particles coming from the vapor-phase collide with the substrate surface.

The developed nanobranched ZnO thin films were successfully exploited for a huge number of applications. By taking advantage of promising electrical and optical properties, in combination with a high specific surface area, the abovementioned porous ZnO layers successfully allowed optimal dye loading, resulting into efficient photoanodes for the fabrication of dye-sensitized solar cells (DSSCs) with a solar conversion efficiency up to 4.58% [38]. The porous and almost isotropic nanobranched network also promoted fast charge transport properties and a good interaction with electrolyte solutions. These factors resulted into superior performances of the porous ZnO matrix when tested in lithium cells for prolonged times, obtaining an almost stable specific capacity higher than 50 $\mu A \cdot h \cdot cm^{-2}$ and high Coulombic efficiencies [39]. On the other hand, photocurrent values up to four orders of magnitude higher than those measured in dark conditions underlined their promising UV sensing capability [40]. Additionally, such porous ZnO films showed encouraging piezoelectric properties [41], especially if compared to those obtained from ZnO thin films showing the more conventional dense microstructure [42]. In particular, upon external mechanical stimulation of the nanobranched ZnO structures, intense piezoelectric output voltage peaks and power density values were achieved, hence suggesting their promising use for sensing and energy harvesting applications [40,42]. The improved piezoelectric behavior was ascribed to the higher defectiveness of the porous structure with respect to the long-range ordered one, typical of dense ZnO thin films. This led to a general reduction in free carrier concentration and mobility, in turn limiting the screening potential and improving piezoelectric voltage generation at the same time. Lastly, the presence of a high porosity and hydrophilic behavior represented the key elements to design a novel synthetic approach for easily obtaining p-type doped nanobranched ZnO structures. In this case, unprecedented ferroelectric, piezoelectric and photovoltaic properties were effectively demonstrated [43].

2.2. Pulsed Laser Deposition

PLD is based on the ablation of a solid source upon interaction with a laser radiation. The ablated species form a vapor phase, condensate on a substrate surface and form the desired thin film after the usual nucleation and coalescence processes. One of the main advantages in using PLD is the possibility to strictly control the chemical composition of the deposited thin film, as the target stoichiometry is more effectively replied than for other PVD methods. However, particulate emission during source ablation strongly affects the performances of this deposition method.

Similar to sputtering, PLD was successfully investigated for growing highly porous ZnO thin films as well. Several works highlighted the importance in using specific oxygen background gas pressures during ablation of the material source, if a porous structure want to be pursued [44–47]. For example, dense and porous ZnO thin films were obtained at room temperature on silicon (Si) substrates in vacuum and in 100 mTorr O_2, respectively. It was found that vacuum deposition formed a dense ZnO layer, while O_2 atmosphere promoted the formation of a porous structure. This last also favored ZnO stoichiometry and the controlled formation of crystal defects like oxygen vacancies, which were almost absent for the vacuum-deposited material. By optimizing the O_2 pressure (66 mTorr) and post-deposition annealing conditions, porous ZnO films made of 100 nm diameter isolated ZnO columns were obtained, showing good crystallinity and strong UV luminescence emission [46]. More recently, the effect of changing the O_2 partial pressure on the porosity of the resulting PLD-grown ZnO thin films was further demonstrated [44]. In this case, Field-Emission Scanning Electron Microscopy (FESEM) and AFM analyses evidenced that small variations of oxygen pressure dramatically changed the resulting thin film morphology from porous ZnO crater-like nanostructures to nanoparticles. The formation process leading to the conversion of pores into nanoparticles as the oxygen pressure increased was effectively demonstrated by the corresponding reduction of surface roughness observed from AFM results. Another study about ZnO thin films grown by PLD discussed the formation of nanopores as a function of the deposition time [48].

This study evidenced how the formation, size and density of these nanopores was influenced by deposition time, due to the different interaction time between the ambient gas and the plasma plume. The growth of pores surrounded by craters was discussed on the basis of the Stranski–Krastanov growth model. All the above-mentioned results are in good agreement with previous observations of ZnO nanoparticles formation during PLD processes and in presence of high oxygen gas pressures. Actually, such nanoparticles allowed the following growth of high aspect ratio ZnO nanostructures by PLD [45]. Similarly, these nanoparticles may be considered as a sort of catalyst promoting the formation of high surface area ZnO thin films.

Alternatively to the use of high O_2 pressure regimes, the glancing angle PLD approach, dealing with a highly oblique incident angle (88°) between rotating ZnO source and Si substrates, allowed the deposition of porous ZnO thin films as well, consisting of 100 nm diameter ZnO posts or helices [49]. The formation of such high surface area network was due to the mutual combination of self-shadowing effects between the ingrowing ZnO structures and substrate rotation speed. In particular, by changing the rotational speed of the substrates from 0.04 to 0.5 rpm, the morphology of the resulting ZnO thin films changed from few isolated helices to vertical posts having 100 nm in diameter. It was also hypothesized that a higher degree of porosity could be achieved by increasing the incident angle. This approach was further exploited to get porous nanostructured ZnO thin films applied to photoelectrochemical cells (PEC) for hydrogen generation from water splitting [50]. To find out the effect of using the oblique-angle deposition, a comparative study on the properties of ZnO thin films fabricated using normal PLD and oblique-angle PLD was carried out. The standard approach resulted into dense thin films with relatively large grain sizes (200 nm), while glancing-angle PLD returned highly porous ZnO structures, made of interconnected spherical nanoparticles of 15–40 nm in diameter. The PEC studies demonstrated that initial photocurrent and hydrogen generation efficiency were strongly influenced by the ZnO thin film morphology, the semiconductor-electrolyte interaction and defect density. In particular, the optimal photon-to-hydrogen efficiency (0.6%) was obtained in the case of the porous morphology obtained by the glancing-angle approach. The improved PEC performances were ascribed to multiple effects, mainly deriving from the presence of a porous network. Firstly, the superior charge transport properties owning to diffusion phenomena taking place from nanoparticle to nanoparticle. Secondly, the decreased oxygen vacancies and Zn interstitials defect density compared to the dense thin film microstructure. Lastly, the large surface-to-volume ratio of the ZnO nanoparticle network, which guaranteed an optimal semiconductor-electrolyte interaction, enhancing the electron-hole separation properties.

The combination of effects from both oxygen-pressure and substrate temperature on the growth of ZnO thin films by PLD was also demonstrated. This approach was exploited to prepare high surface area, three dimensional (3D) ZnO nanowall networks with a nest-like structure, shown in Figure 4 [51]. The nanowall structure was obtained by a two-step PLD process. This involved first the deposition of a thin ZnO seed layer at a substrate temperature of 300 °C and O_2 pressure of 10 mTorr. Then, the 3D nanowall ZnO network was obtained at 550 °C and O_2 pressure of 500 mTorr. The nest-like structures were composed of a network of remarkably uniform and interconnected nanowalls, whose average thickness was around 15 nm (Inset A of Figure 4). AFM characterization also revealed that about 80% of the depths of the nanowall was 70 nm (Inset B of Figure 4). The formation of such particular 3D structure was explained in terms of a vapor–solid model. According to this, a templating/seeding effect due to self-nucleation directly occurred on the substrate surface during the beginning of the growth, at low temperature and low O_2 pressure conditions. Then, formation of the 3D ZnO nanowall network was promoted by the following high substrate temperature and high O_2 background regime.

Concerning again the effect due to different substrate temperatures and oxygen partial pressure values during PLD growth, a parametric study on the resulting morphologies, optical and structural properties was carried out [52]. Regarding the deposition time, ZnO nanowalls were obtained at different period of times of 5, 7, 10, 15, and 45 min. Figure 5a shows that formation of ZnO nanoparticles (average size 40–390 nm) randomly distributed on the substrate surface occurred after

5 min. Then, coalescence phase was observed after 7 min while two-dimensional ZnO nanowalls were grown vertically after 10 min. In this case, the average pore size was between 50 and 140 nm and the walls between the honeycombs showed a uniform thickness of around 50 nm.

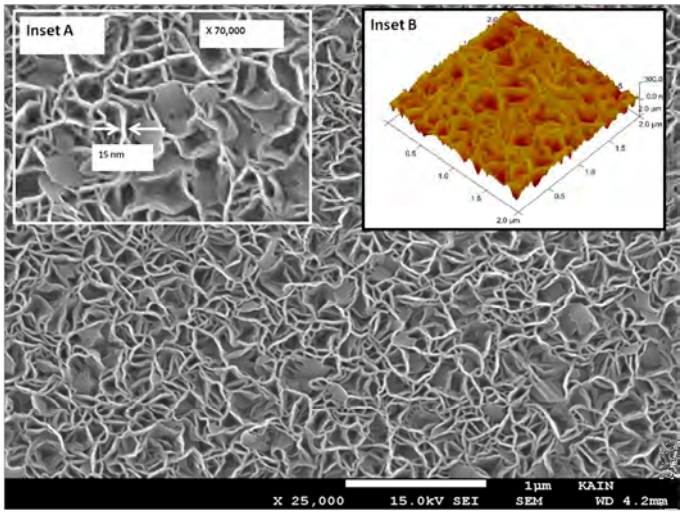

Figure 4. Low-magnification scanning electron microscope image and atomic force microscope profile of the 3D ZnO nanowall network grown vertically on Si(100) at 550 °C under 0.5 Torr O_2 background pressure. Scale bar is 1 µm. Reproduced with permission from [51]; Copyright 2015 Elsevier.

Similarly, crystalline ZnO thin films with a tunable porosity and anisotropic structure were prepared by changing the O_2 pressure (from 100 mTorr to 400 mTorr), during PLD fabrication process [53]. The resulting films were tested as photoanodes for the fabrication of glass-based and flexible, polymer-based DSSCs. By selecting the most appropriate O_2 pressure value (300 mTorr) and thickness (10 µm), high surface area ZnO films were obtained. This allowed for an optimal dye loading, prolonged electron lifetime and enhanced electrolyte diffusion through the crystalline porous ZnO framework, resulting into better photovoltaic behaviors and improved conversion efficiencies (up to 3.89%) under light illumination. Another PLD parameter affecting the porosity of ZnO thin films is pulse duration. This was effectively demonstrated by using a laser (λ = 810 nm, laser fluence 2 J·cm^{-2}) with different pulse durations of 50 fs, 200 fs, 1 ps and 10 ps. In such cases, porous ZnO films were obtained, with a degree of porosity decreasing for longer pulse durations [54].

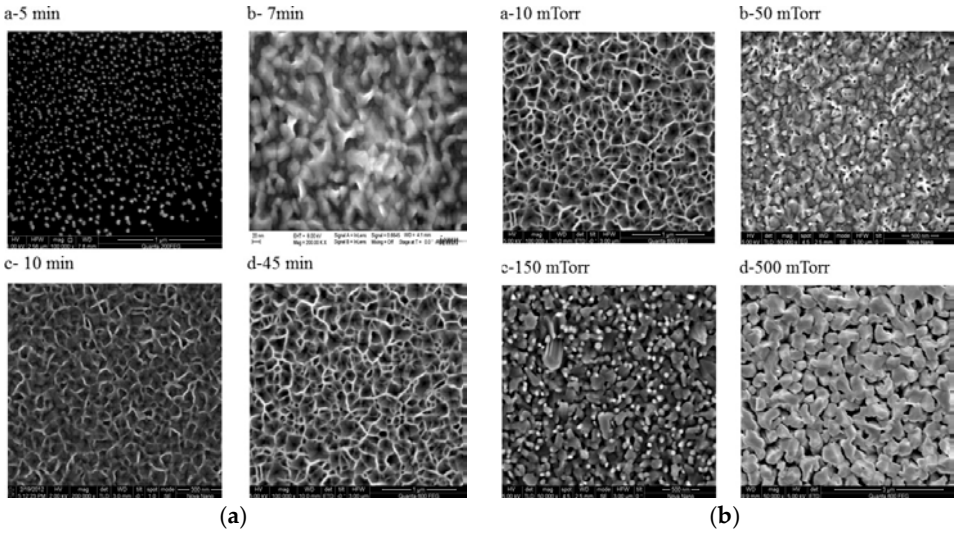

Figure 5. *Cont.*

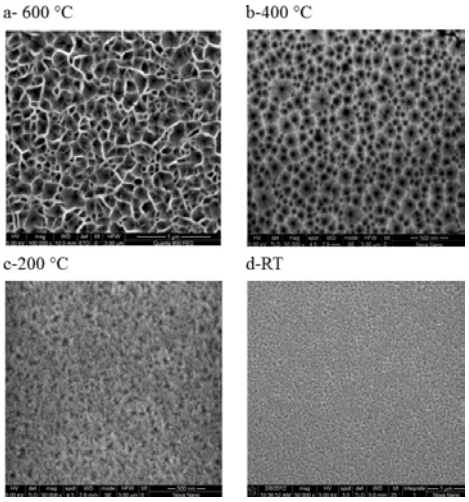

(**c**)

Figure 5. Scanning Electron Microscope images showing the effect of (**a**) deposition time, (**b**) oxygen pressure, and (**c**) substrate temperature on the morphology of the resulting ZnO nanowall network. Adapted with permission from [52]; Copyright 2014 Elsevier.

3. Chemical Deposition of Porous ZnO Thin Films

3.1. Spray Pyrolysis

Spray pyrolysis is a well-established technique used for preparing high-quality thin and thick ZnO films in a very simple, cheap and easy way. This synthetic approach allows for growing both dense and porous films, as well as powdered materials. The process roughly consists in three steps: atomization of a metal salt precursor solution, transportation of the resulting vapors, condensation of the drops and their thermal decomposition on a heated substrate. The formation of a thin film network is then obtained by the superimposition and overlap of the metal salt drops over the substrate surface, and their conversion into oxides by heating of the substrate. The main parameters affecting the final thin-film structure and properties are the solvent, type of salt and concentration, and additives present in the precursor solution.

Porous crystalline ZnO films obtained by spray pyrolysis have been reported in numerous cases. The precursor solution generally consists of zinc acetylacetonate [55], zinc nitrate [56], or zinc acetate dehydrate [57,58] salts dissolved in aqueous solution. In all the cases it was found that both the use of different precursor concentrations, substrate temperatures or post-deposition thermal annealing treatments strongly influenced the resulting film morphology, photoconductive and photoluminescent properties [56–60]. The porous ZnO structures resulting from spray pyrolysis method generally showed good electrical conductive properties and light transparency. These aspects, coupled to optimal dye absorption properties, demonstrated their promising use as photoanodes in DSSCs fabrication [55]. Moreover, their application as blocking layer (BL) in standard TiO_2-based solar cells has been successfully reported; the presence of spray-pyrolysis derived porous ZnO BL effectively reduced charge carrier recombination phenomena, improving the cell efficiency more than 20% with respect to cells efficiencies obtained without the BL [61]. Most of the applications based on ZnO films obtained by spray pyrolysis also rely on the fabrication of gas sensors. Several works gave evidence of their promising use as gas sensors for the detection of various gas species, including acetaldehyde [62], ammonia [63,64] and H_2S [65]. In these cases, the room temperature sensing characteristics showed that gas concentrations ranging from hundreds of ppm up to few ppm could be successfully detected with good selectivity and fast response/recovery times. In addition, other gases like methanol, ethanol, 2-propanol, benzyl alcohol and acetone were considered, further proving the best selectivity of such porous ZnO structures towards those abovementioned gases [62,63,66].

Another promising application of spray pyrolysis technique is the easy preparation of multifunctional doped ZnO films with a porous structure. In this case, doping can be achieved by simply including an additional doping precursor within the synthesis solution, such as aluminum chloride, tin chloride and silver nitrate. This approach was explored to successfully dope porous ZnO with various elements, including Al [67,68], Sn [69], Ag [70], Na [71], Mg [72] and many others [73,74]. Similarly to pristine ZnO, the resulting doped structures were found to be highly promising in view of gas sensors fabrication, especially for ammonia and H_2S detection. Actually, transition metal doping (Co, Cu, Ni) was proved as an effective way to achieve gas sensing properties with improved response and selectivity [75]. The H_2S sensing property and selectivity of Ti-doped ZnO thin films was investigated as well. The influence of Ti doping concentration on H_2S detection was considered, finding that 2 wt.% Ti-doped ZnO thin films showed the maximum response (~0.29) to 20 ppm H_2S exposition at 200 °C [74]. In a similar way, H_2S sensing properties of Cu-doped ZnO thin films (1–4 wt.%) were also demonstrated [76]. In this case, the best response (~0.38) towards 20 ppm H_2S at 523 K operating temperature was achieved for the 4 wt.% Cu-doped ZnO. Ni-doped and V-doped ZnO thin films featuring similar sensing capabilities were demonstrated too [77–79]. The acetone gas sensing tests performed on Ni-doped ZnO highlighted a good sensing response for acetone concentration as low as 116 ppb, with response and recovery times of about 6 s and 2 s, respectively [79]. Concerning V-doped ZnO, gas testing analyses gave evidence of good sensing response in a wide range of operating temperatures (from 350 °C to 300 °C) towards 100 ppm of acetone, 50 ppm of ethanol and 500 ppm of H_2. Furthermore, a maximum response of 100 was achieved for acetone 100 ppm at 450 °C [80]. Alternatively, good ammonia sensing properties were achieved for porous Mg-doped ZnO thin films, with the lower Mg-doping concentration showing the best performances, with quick response and recovery times at room temperature [81].

Other successful applications for doped ZnO films obtained by spray pyrolysis were expressed in terms of their improved photocatalytic efficiencies and electrical properties, resulting into their successful application as photocatalyst [82,83] and as photoanodes in DSSCs fabrication [84]. Finally, In-doped and Sn-doped ZnO thin films also showed very interesting antibacterial properties against *Staphylococcus aureus* [85,86], with better antibacterial activities found by increasing the doping concentration.

3.2. Electrodeposition

Electrochemical deposition, also called electrodeposition, is a versatile, low cost, easy and scalable method, particularly useful for growing highly porous ZnO thin films at relatively low working temperatures (generally lower than 100 °C). This method deals with the use of charged reactive species diffusing through a solution, under the application of an external electric field. Electrodeposition is carried out in a three-electrode electrochemical cell, composed by a reference electrode (Ag/AgCl), the counter electrode (platinum wire or sheet), the working electrode and the electrolyte solution. The application of a constant voltage between the electrodes allows the diffusion of reactive species within the electrolyte solution.

Depending on several deposition parameters, like the applied voltage, deposition time, charge density and solution precursor, the porosity and morphology of electrodeposited ZnO films may be tuned, accordingly. For example, it has been reported that the growth rate of ZnO films showing different porosities and morphologies prepared by cathodic electrodeposition was influenced by sodium laurylsulfate concentration. This surfactant was added to the growth solution, made of aqueous oxygen saturated zinc chloride and other organic acids. If sodium laurylsulfate concentration was high enough, formation of micelles and their assembly on the charged electrode surface could be achieved, allowing for the formation of the porous structure, but also leading to a strong increase in the current density and finally, to the growth rate [87]. The promising optical and electrical properties of porous ZnO films obtained by electrodeposition have been reported in numerous cases [88–90]. In particular, it was found that enhanced photocurrent values were due to a combination of multiple effects,

dealing with improved visible absorption properties, optimization of oxygen defects within the crystal structure, and finally the presence of an appropriate porous surface morphology, allowing for the incoming light to more effectively generate multiple reflections and diffusion scattering effects before being emitted, finally increasing the ZnO solar light absorption properties [89]. Such a pronounced photocurrent, coupled with a porous morphology, was successfully exploited for the fabrication of sensors and DSSCs [90]. Also in this case, the addition of surfactants during ZnO electrodeposition turned out to be an effective way for inducing high porosities and fast growth rates. The resulting porous samples displayed a persistent photoconductive behavior, which conductivity transients of several hours in dry atmosphere, independently of illuminating conditions. More interestingly, the photoconductive behavior was observed even when illuminating with low-bandgap energy light. This property was explained in terms of lattice relaxation processes involving surface states within the ZnO bandgap, which favored capture of electrons immediately after photoexcitation phenomena. Similar photoconductive properties were explored also for the fabrication of flexible photosensors [88]. In this case, fast photo-response (0.821 s) and recovery times (1.257 s) were obtained under solar light irradiation, together with a large on/off current density ratio (65.94). Again, such promising results were mainly due to the porous ZnO network, able to provide more convenient photoelectron pathways and additional reaction sites for photocurrent generation.

Exploiting the promising photoelectrical properties of electrodeposited porous ZnO films, several works demonstrated their effective application as photoanodes in DSSCs fabrication. This was proved by Chen et al. [91], who prepared porous ZnO electrodes by cathodic electrodeposition from an aqueous zinc nitrate solution, also containing polyvinylpyrrolidone (PVP) as surfactant. Morphological and structural characterization showed that the porous framework was made of hexagonal wurtzite crystalline grains in the 20–40 nm range. Taking advantage of the film porosity and crystallinity, coupled to the optimization of the final photoanode thickness (8 μm), DSSCs showing conversion efficiencies as high as 5.08% were obtained. In another case, the promising properties of squaraine-sensitized mesoporous ZnO electrodes were expressed in terms of larger photocurrent generation and solar-to-energy conversion efficiencies in comparison with those obtained from standard TiO_2-based electrodes sensitized with the same dye molecule [92]. Electrodeposition of nanoporous ZnO films were successfully deposited on conductive nanofibers as well, and tested in DSSCs [93]. Prior to deposition of the porous matrix, a compact ZnO BL was electrodeposited, in order to suppress charge carrier recombination at the interface with the conductive support. Then, during the same electrodeposition process, porous ZnO structures were grown by including Eosin Y as a pore-creating additive in the electrochemical bath.

The addition of Eosin Y agent to electrodeposition found use also in view of photocatalytic degradation applications. In particular, the deposition time and the Eosin concentration were optimized to get mesoporous ZnO thin films with large internal surface areas and good mechanical properties [94]. The photodegradation rate of methylene blue (MB) and Congo Red molecules were maximized with Eosin concentrations higher than 40 μM. Since the photodegradation behavior was found to be promoted in the case of the large-diameter pores, the development of narrower pores (8 nm) did not enhance further the ZnO photocatalytic performance. Another approach for the development of porous ZnO films with good photocatalytic properties was the electrodeposition of metallic Zn coatings on mild carbon steel sheet in sulfate bath by DC current, and their subsequent thermal oxidation in air at temperatures ranging between 400 °C and 800 °C [95]. In another work, the influence of annealing conditions of electrodeposited Zn films on the resulting photocatalytic activities were studied again in terms of MB photodegradation under UV light. The ZnO films showed good photodegradation efficiency and photostabilization, especially for the samples annealed at 500 °C for 4 h [96]. With this particular set of annealing conditions, uniform intertwining-rod structures were formed, showing around 100% photodegradation efficiency and good photostabilization following three successive growth reaction cycles. The observed superior properties were due to the large effective area present in the so-formed ZnO structures, which provided more active

sites for radical-organic interactions and effective interfacial charge transfer, finally resulting into better photocatalytic activities. The effect of thermal oxidation at 800 °C on the morphology of electrodeposited ZnO films was further considered. Improved photocatalytic degradation of MB was obtained due to additional morphological effects deriving from the oxidation process, which led to better oxidation conditions but more strikingly, to the rise of high surface area, columnar needle or rod like ZnO morphologies. By controlling various deposition parameters, like the applied potential (in the range −0.9 ~−1.1 V), the electrodeposition duration (from 1800 to 7200 s) and times (from 1 to 6), a direct method was implemented to grow porous ZnO nanorod arrays (ZNRAs) featuring different morphologies, on stainless steel mesh substrates [97]. The photocatalytic degradation of Rhodamine-β under UV light irradiation was investigated. The results are shown in Figure 6, highlighting how the degradation efficiency could be highly improved from 89.4% to 98.3% if deposition times increased from one to six. This was mainly due to the higher amount of ZnO catalyst deposited onto the steel mesh, hence resulting into higher photocatalytic efficiencies. Alternatively, electrochemical deposition allows the formation of ZnO nanosheets on pre-seeded substrates. Similar to porous ZnO thin films, the prepared nanosheet array demonstrated promising MB photodegradation properties under visible-light irradiation. In particular, the degradation efficiency could reach 90% after 180 min, and was 1.5 times better than for commercial ZnO powders [98].

Due to the high specific surface area of electrodeposited ZnO thin films, conductive hydrophobic or even superhydrophobic surfaces were prepared as well. Superhydrophobicity could be achieved directly [99] or even by post-synthesis chemical modification treatments on the prepared ZnO surfaces [99,100]. In particular, Lin et al. [99] succeeded in preparing biomimetic self-cleaning ZnO surface on steel substrates, by coupling the electrodeposition of metallic Zn films on steel substrates, the consequent hydrothermal growth of low-dimensional ZnO structures (contact angle of 137.85°) and finally, their surface modification with low-surface-energy chemical moieties (contact angle 157.59°).

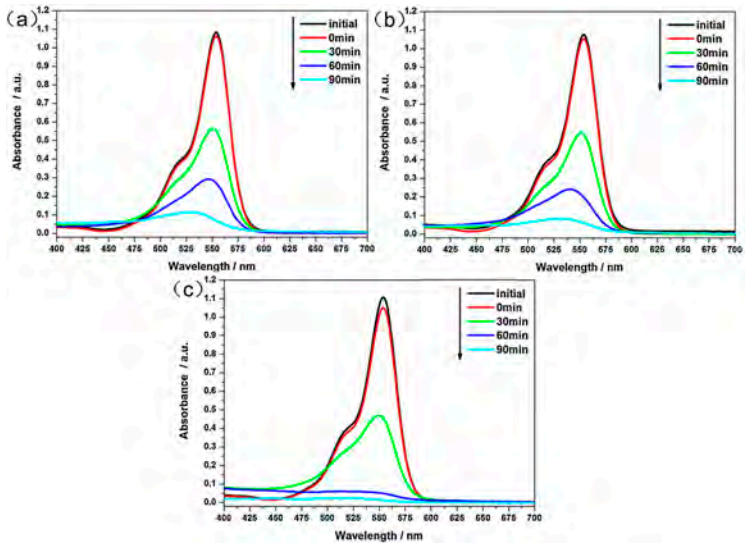

Figure 6. Absorbance spectra of Rhodamine-β dye aqueous solutions under UV irradiation, in presence of ZnO nanorod arrays (ZNRAs), synthesized for different electrodeposition times: (**a**) one time; (**b**) three times; and (**c**) six times. Reproduced with permission from [97]; Copyright 2014 Elsevier.

3.3. Sol-Gel Assisted Methods

Sol-gel assisted methods have been explored as cheap and simple alternative synthetic techniques to get porous ZnO thin films. These include spin-coating [101], dip-coating [102], hydrothermal routes [103] and chemical bath deposition (CBD) [104–106]. The sol-gel approach first deals with the preparation of a colloidal solution combining zinc precursor powders (zinc acetate dihydrate, zinc nitrate hexahydrate or zinc chloride) and bases (sodium hydroxide), both mixed in organic

solvents (ethanol, methanol or 2-propanol). The addition of hexamethylenetetramine to the solution is also widely recommended, since it promotes ZnO crystallization and allows for a strict control over the final ZnO morphology. The prepared solution is stirred for few hours at mild conditions (60–70 °C) and finally deposited on the desired substrates. To further promote ZnO crystallization as well as the formation of the desired porous morphology, a final sintering process is generally performed for several hours at temperatures ranging between 300 °C and 500 °C.

Sol-gel derived porous ZnO structures show high surface areas (see Figure 7) coupled with the existence of good optical and electrical properties. All these aspects result into interesting application properties. For example, porous ZnO obtained by CBD exhibited good sensing properties against a wide range of toxic and combustible gases like hydrogen, liquid petroleum gas, methane and H_2S. The response of the ZnO thin film sensors was found to be significant, even for low gas concentrations, i.e., 50 ppm for methane, 15 ppm for H_2S [104]. Highly porous ZnO thin films prepared by a sol–gel approach showed promising photocatalytic properties, efficiently promoting the aqueous solution decomposition of phenol, chlorophenol, naphthalene and anthracene to CO_2 [101]. Similar promising results were observed also for porous ZnO structures grown on alumina substrates. In this case, different morphologies (from nest-like to globular shape ones) were investigated and the resulting photocatalytic properties expressed in terms of Methyl Orange degradation. The highest photocatalytic activity was obtained for porous ZnO films sintered at 500 °C and showing successive nest-like structures [107]. The growth of highly porous ZnO by sol-gel approach was also applied in the pores of anodic alumina matrices having tens of μm in thickness, followed by thermal treatment [108,109]. Lamellar-like morphology, high surface areas (between 99 and 198 $m^2 \cdot g^{-1}$) and pore volumes (0.35 and 0.1 $cm^3 \cdot nm^{-1} \cdot g^{-1}$) were obtained for ZnO nanostructures into alumina. In some cases, however, the partial alumina dissolution during the synthesis process led to highly porous membrane with mixed phases of wutzitic ZnO and γ-Al_2O_3. The sol-gel method was also successfully applied to the preparation of highly porous ZnO films for CO gas sensing applications. By changing the calcination temperature, different morphologies and gas sensing responses were possible, with the best sensing response achieved for a calcination temperature of 500 °C [110]. Hierarchically, 3D porous ZnO structures were obtained by hydrothermal method as well [103]. The analyses of both ethanol and methanol gas sensing properties demonstrated that hierarchically porous structures highly improved the gas sensing performances with respect to commercial ZnO powders. This was due to the high porosity and three-dimensional morphology, as making easier gas diffusion and transport within the sensing material. More recently, mesoporous ZnO film structures were obtained by CBD, following a green organic-solvent-free route. The high specific surface area of the prepared ZnO structures (19–66 $m^2 \cdot g^{-1}$) allowed efficient drug loading and release, thereby highlighting the ability of mesoporous ZnO structures to work as promising drug delivery carriers [111].

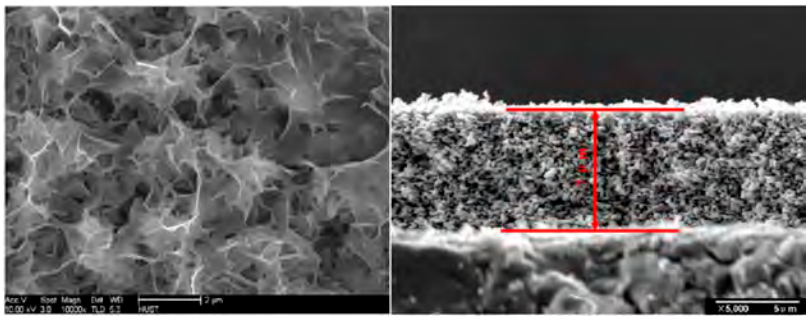

(**a**) (**b**)

Figure 7. Examples of porous ZnO morphologies obtained by sol-gel methods. (**a**): a typical FESEM image of ZnO thin solid films deposited via a modified chemical bath deposition method. Scale bar is 2 μm. Reproduced with permission from [106]; Copyright 2006 Elsevier. (**b**): Cross-section FESEM image of ZnO films prepared at 0.05 mol/L methanolic zinc acetate solution and sintered at 500 °C. Scale bar is 5 μm. Reproduced with permission from [107]; Copyright 2005 Elsevier.

4. Template-Assisted Methods

Porous ZnO thin films have been also prepared by template-assisted methods. In these cases, the macro/microporous framework is given by the use of template agents with suitable geometries. Once ZnO deposition on the pre-treated substrates is completed, the template is removed, leaving the desired ZnO porous framework.

Three-dimensional polystyrene (PS) opal [112,113] and polyethylene glycol [114] have been proposed as organic template to obtain two-dimensional or three-dimensional porous ZnO structures. In the first case, PS spheres were dispersed on conductive glass substrates using the vertical deposition technique, resulting in the formation of PS opal films covering the substrate surface (see Figure 8a). Then, the PS-coated substrates were used as electrode in a three-electrode cell configuration, also containing a Zn plate and the electrolyte solution (0.04 M $Zn(NO_3)_2$ in water or mixed ethanol–water solvents). The deposition process was carried out for 40 min or 2 h at 62 °C and the reference voltage was kept at −0.96 V vs. reference electrode. After electrodeposition, the PS template was thermally or chemically removed, leaving the long-range ordered porous ZnO framework shown in Figure 8b,c. By exploiting again the combination of electrodeposition and PS templates, ordered porous ZnO films were obtained on conductive indium-tin-oxide glass substrates [115]. The influence of electrolyte concentration (zinc nitrate aqueous solution) on the current density, growth rate and the resulting film morphology were mostly investigated. For higher electrolyte concentrations, the deposition rate was higher, accordingly. This resulted into a better filling of the template structure, finally giving a more robust porous ZnO film, without showing cracks or deformation after removing the PS template. In a similar way, porous ZnO layers were successfully obtained on PS template glass substrates by dip coating method [116]. In this case, the influence of ZnO sol concentration and dipping time on the morphology of the resulting ZnO porous structures was pointed out, showing a shrinkage ratio of about 30% from pore to PS in the optimal synthesis conditions.

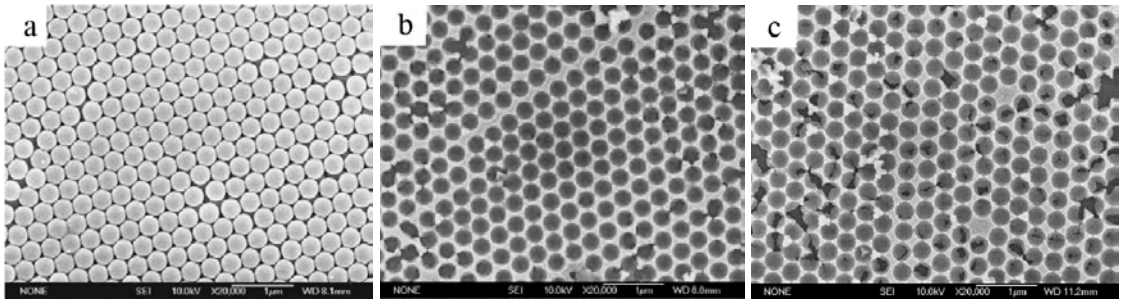

Figure 8. (**a**) A typical SEM image of the original PS opal templates. (**b**,**c**) SEM images of the 2D ordered ZnO porous films at different deposition times of (**a**) 40 min and (**b**) 2 h. Adapted with permission from [113]; Copyright 2005 Elsevier.

In addition, it was highlighted how the electrostatic potential could affect the quality of the fabricated porous ZnO structures. For low electrodeposition potential values (1 V) the growth rate of ZnO crystals on the substrate was slow, allowing to sufficiently fill the interstices among PS spheres. This led to hemi-spherical hollow arrays after 2 h deposition and removal of PS template. On the contrary, at a higher potential (1.4 V) the crystallites grew rapidly and could not fully fill the interstices, resulting in a nanowall-like structure. Therefore, the control over the deposition potential allowed to change the pore morphology from hemispherical to a well-like structure [117]. More recently, patterned spherical nanoshells of ZnO were obtained for the first time [118], using an array of PS spheres prepared by self-assembly method and 80 nm-thin ZnO layer deposited onto PS array by a drop-coating method. The PS array was immersed in a zinc precursor solution for several times, until the final ZnO thickness was achieved. Then, calcination was performed to stabilize the coating and to promote ZnO crystallization. Finally, PS sphere template was thermally removed, allowing the

formation of nanoshell ZnO structures with clear evidence of internal voids. The UV-visible light absorption properties were highly improved due to the formation of this spherical ZnO nanoshell cavities. The combination of PS opal templates with ZnO thin films was obtained also in other cases. ZnO thin films deposited by RF magnetron sputtering led to the fabrication of three dimensional core-shell ZnO photonic crystals [119]. The PS template allowed the porous structure and formation of cavities to be properly controlled, positively affecting the resulting photonic band gap properties. Wet infiltration of PS opal templates with ZnO precursors also produced ZnO inverse-opal films with improved photodetecting properties, showing excellent selectivity and reversible response to optical switch [120]. Three-dimensionally ordered, macroporous ZnO structures were obtained as well [121]. Due to the high surface area (18.7–34.5 $m^2 \cdot g^{-1}$), the macroporous structure was successfully proposed as ethanol sensor, showing good sensitivity, selectivity and electron transfer properties. In a similar preparation method, multilayered porous ZnO thin films were obtained and tested as NO_2 gas sensor under UV light irradiation [122]. The film porosity positively influenced the ever-decaying light intensity or ever-decreasing photogenerated carriers, finally maximizing the film response when interacting with NO_2 gas. Nanopatterned ZnO cavity-like structures were obtained as well, by the combination of hydrothermal synthesis of ZnO together with the use of PS opal template and nanosphere lithography technique [123]. p-n heterojunctions were then fabricated using copper oxide as p-layer, and the corresponding photoelectric conversion efficiencies evaluated. In comparison to the use of planar ZnO layers, the presence of a high-surface area ZnO cavity-like structure effectively improved the charge carrier collection within the heterojunction.

Atomic Layer Deposition (ALD) is well known for its ability to coat complex 3D substrate geometries in a conformal way. This peculiarity, in combination with the use of PS template substrates, was recently proved as an effective way to get micrometer-thick 3D mesoporous ZnO networks, showing a periodic gyroid structure or a random worm-like morphology as well. The presence of a mesoporous structure, with an average pore size of 30 nm, was confirmed for both the geometries, which are shown in Figures 9 and 10. Such mesoporosity was found to be the ideal condition for promoting exciton dissociation in hybrid photovoltaic devices. This was successfully demonstrated in the case of the worm-like morphology, which was integrated into a hybrid P3HT/ZnO hybrid photovoltaic device. The presence of the mesoporous 3D worm-like ZnO structure effectively resulted in improved short-circuit current density values [124].

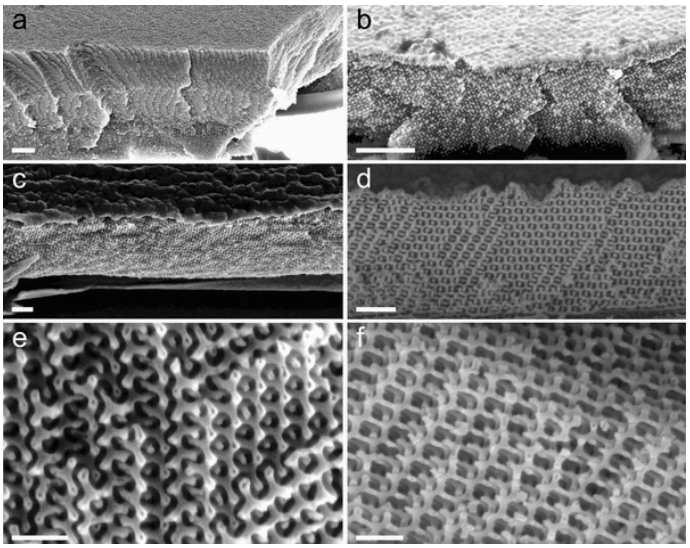

Figure 9. Side-view SEM images at a 45° angle of gyroid replication into ZnO: (**a**) gyroid PS template; (**b**) as-deposited ZnO-PS hybrid; (**c**) ZnO gyroid after annealing at 550 °C; (**d**–**f**) different faces of the ZnO gyroid shown in (**c**). Scale bars are 1 μm for panels (**a**,**b**), 400 nm for (**c**,**d**), 200 nm for (**e**,**f**). Reproduced with permission from [124]; Copyright 2014 John Wiley & Sons, Inc.

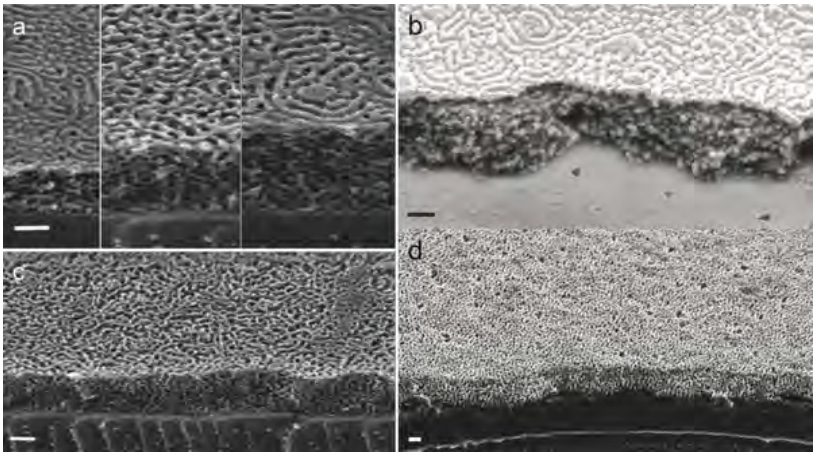

Figure 10. SEM of ZnO replication of the worm-like morphology: (**a**,**c**) worm-like PS template; (**b**) as-deposited ZnO-PS hybrid; (**d**) ZnO morphology after annealing at 400 °C followed by etching of the top compact layer. Scale bar are 200 nm. Reproduced with permission from [124]; Copyright 2014 John Wiley & Sons, Inc.

5. Others

Apart from PVDs, chemical synthetic methods and template-assisted approaches, other works demonstrated that porous ZnO thin films may be easily obtained by following alternative synthetic routes/technological fabrication processes. Yong et al. exploited the oxidative action of femtosecond laser radiation to design a simple, one-step fabrication method leading to ZnO layer made of hierarchical micro- and nano-structures [125]. This was achieved by femtosecond laser ablation of a metallic Zn layer. The resulting laser-ablated Zn surface showed switchable wetting properties between superhydrophobic and quasi-superhydrophilic states upon UV irradiation and dark storage, respectively. The observed switchable properties were ascribed to the dual effect of the ablation process, which induced oxidation of the Zn surface and promoted the formation of a hierarchical rough microstructure at the same time. An alternative way to get hierarchical ZnO structures was achieved by a simple oxidation of metallic Zn films in hot water at 90 °C [126]. By changing the oxidation time, a huge amount of various morphologies could be obtained and ranging from pencil-like nanorods (6 h), to nanotubes (16 h) and lotus-like (24 h) structures. The occurrence of different morphologies as a function of the oxidation time was explained in terms of specific electrochemical reactions occurring at the Zn surface, each one predominating on the others as long as ZnO micro/nanostructures were going to be formed. The most interesting and promising ZnO structures were the lotus-like ones; when tested in hybrid organic–inorganic solar cells, a power conversion efficiency as high as 1.18% was achieved. Alcaire et al. successfully showed the fabrication of porous ZnO layers by the combination of vacuum- and plasma-assisted processes. In the first step, Zn-phthalocyanine (ZnPc) solid precursor was sublimated in vacuum conditions, leading to the formation of polycrystalline films rather than single crystal ZnPc nanowire arrays. Then, oxygen plasma treatment was used to oxidize the starting ZnPc film and to form the porous structure [127]. At very high substrate temperatures and/or for prolonged times, the complete conversion from ZnPc to ZnO could be achieved. In this way, highly porous ZnO thin films with surface coverage as low as 55% were obtained. Such a reduced density resulted into an extremely low refractive index ($n_{(550\ nm)}$ = 1.11) for an optical thickness of 135 nm, being one of the lowest refractive index ever reported for ZnO. This might open the way to possible applications of such porous ZnO films as antireflective coatings and for graded-index multilayer systems. The anodic oxidation technique was also investigated [128]. Metallic Zn sheets were set as anodes in a three-electrode electrochemical cell apparatus, containing a 3% phosphoric acid in ethanol. Then, oxidation was performed by applying a constant voltage of 15 V for different times, ranging from 5 min to 2 h. In this way, porosity of ZnO films was tuned accordingly.

The cytotoxic effects of the prepared ZnO films were investigated, demonstrating the existence of a pore density-dependent cytotoxic behavior against fibroblast cells.

6. Conclusions and Future Outlooks

The main achievements in the synthesis of high-surface areas, porous ZnO thin films are summarized in Table 1. Various porosities of different size and cavity shapes may be successfully achieved by exploiting several deposition techniques. Sputtering and electrodeposition generally provide a mesoporous ZnO structure, while pulsed laser deposition, spray pyrolysis, electrodeposition and sol-gel ones often allow for different types of porosity, ranging from the meso- up to the macro-scale.

Table 1. Synthesis method, porous structure characteristics and final applications of porous zinc oxide thin films.

Synthetic Approach	Porous Structure			Ref.
	Type of Porosity [1]	Pore Size, Specific Surface Area (SSA)	Analyses Methods	
Sputtering	Meso	4 nm	AFM	[32]
	Macro/Meso	<100 nm	FESEM, HRTEM	[33]
	Macro/Meso	50–100 nm	FESEM	[35]
	Meso	~27 nm, SSA 14 $m^2 \cdot g^{-1}$	FESEM, N_2 adsorption	[43,129]
Pulsed laser deposition	Meso	<50 nm	FESEM, AFM	[44]
	Macro	113–184 nm	FESEM, AFM	[48]
	Macro	50–140 nm	SEM	[52]
	Macro/Meso	10–100 nm	FESEM	[53]
Spray pyrolysis	Macro	~100 nm	FESEM	[64]
	Meso	10–25 nm, SSA 28.88 $m^2 \cdot g^{-1}$	N_2 adsorption	[79]
Electro deposition	Meso	10–20 nm	FESEM	[92]
	Meso	<50 nm	SEM, TEM	[93]
	Meso	<8 nm, SSA 20–140 $m^2 \cdot g^{-1}$	Kr adsorption	[94]
Sol-gel	Meso	~7 nm, SSA 37.47 $m^2 \cdot g^{-1}$	N_2 adsorption	[103]
	Macro	~100 nm	FESEM	[105]
Template-assisted	Macro	>1 µm	FESEM	[112,113,116,117]
	Meso	30 nm	FESEM	[124]

[1] According to IUPAC notation.

Independently of the particular synthetic approach, the prepared porous ZnO films found successful application for the fabrication of photoanodes for DSSCs, the photocatalytic degradation of various dye molecules, and for the fabrication of gas sensors. In the specific case of spray pyrolysis, this method turned out to be the most successful and simple methods to easily synthesize doped ZnO thin films with a porous structure. As an alternative to the methods mentioned above, template-assisted methods successfully allowed for the growth of three dimensional porous ZnO structures, also showing very complex 3D geometries. In most of the cases, polystyrene opals have been definitely proved as the most promising sacrificial template useful to confer the desired macro/microporosity after ZnO deposition.

New future applications could be envisioned for porous ZnO thin films, thanks to the combination of the following aspects: (i) very interesting ZnO properties, i.e., antibacterial activity, piezoelectricity and biocompatibility; (ii) the existence of mesoporous/macroporous structures with high surface areas; (iii) the use of thin-film-based technologies, allowing for the preparation of large-area substrate materials in a controllable and repeatable way. Actually, the existence of mesoporous ZnO thin films would allow for several drugs and biologically relevant molecules to be loaded and delivered,

hence opening the way to the application of porous ZnO structures for drug-delivery systems. On the other hand, macroporous ZnO structures showing good antibacterial and piezoelectric activities might allow for the design of new piezoelectric-active scaffold materials for tissue engineering applications.

Author Contributions: Marco Laurenti and Valentina Cauda jointly conceived the topic and outline of the manuscript; Marco Laurenti wrote the paper; Valentina Cauda supervised the overall writing of the manuscript.

Conflicts of Interest: The authors declare no conflict of interest.

References

1. Zhu, P.; Weng, Z.Y.; Li, X.; Liu, X.M.; Wu, S.L.; Yeung, K.W.K.; Wang, X.B.; Cui, Z.D.; Yang, X.J.; Chu, P.K. Biomedical applications of functionalized ZnO nanomaterials: From biosensors to bioimaging. *Adv. Mater. Interfaces* **2016**, *3*, 1500494. [CrossRef]
2. Laurenti, M.; Cauda, V. ZnO nanostructures for tissue engineering applications. *Nanomaterials* **2017**, *7*, 374. [CrossRef] [PubMed]
3. Janotti, A.; Van de Walle, C.G. Fundamentals of zinc oxide as a semiconductor. *Rep. Prog. Phys.* **2009**, *72*, 126501. [CrossRef]
4. Djurisic, A.B.; Leung, Y.H. Optical properties of ZnO nanostructures. *Small* **2006**, *2*, 944–961. [CrossRef] [PubMed]
5. Yu, J.G.; Yu, X.X. Hydrothermal synthesis and photocatalytic activity of zinc oxide hollow spheres. *Environ. Sci. Technol.* **2008**, *42*, 4902–4907. [CrossRef] [PubMed]
6. Laurenti, M.; Porro, S.; Pirri, C.F.; Ricciardi, C.; Chiolerio, A. Zinc oxide thin films for memristive devices: A review. *Crit. Rev. Solid State Mater. Sci.* **2017**, *42*, 153–172. [CrossRef]
7. Wang, Z.L. Zinc oxide nanostructures: Growth, properties and applications. *J. Phys. Condens. Matter* **2004**, *16*, R829–R858. [CrossRef]
8. Laurenti, M.; Stassi, S.; Lorenzoni, M.; Fontana, M.; Canavese, G.; Cauda, V.; Pirri, C.F. Evaluation of the piezoelectric properties and voltage generation of flexible zinc oxide thin films. *Nanotechnology* **2015**, *26*, 215704. [CrossRef] [PubMed]
9. Cui, J.B. Zinc oxide nanowires. *Mater. Charact.* **2012**, *64*, 43–52. [CrossRef]
10. Li, J.Y.; Chen, X.L.; Li, H.; He, M.; Qiao, Z.Y. Fabrication of zinc oxide nanorods. *J. Cryst. Growth* **2001**, *233*, 5–7. [CrossRef]
11. Dumontel, B.; Canta, M.; Engelke, H.; Chiodoni, A.; Racca, L.; Ancona, A.; Limongi, T.; Canavese, G.; Cauda, V. Enhanced biostability and cellular uptake of zinc oxide nanocrystals shielded with a phospholipid bilayer. *J. Mater. Chem. B* **2017**, *5*, 8799–8813. [CrossRef]
12. Cauda, V.; Pugliese, D.; Garino, N.; Sacco, A.; Bianco, S.; Bella, F.; Lamberti, A.; Gerbaldi, C. Multi-functional energy conversion and storage electrodes using flower-like zinc oxide nanostructures. *Energy* **2014**, *65*, 639–646. [CrossRef]
13. Soci, C.; Zhang, A.; Xiang, B.; Dayeh, S.A.; Aplin, D.P.R.; Park, J.; Bao, X.Y.; Lo, Y.H.; Wang, D. ZnO nanowire UV photodetectors with high internal gain. *Nano Lett.* **2007**, *7*, 1003–1009. [CrossRef] [PubMed]
14. Jiang, C.Y.; Sun, X.W.; Lo, G.Q.; Kwong, D.L.; Wang, J.X. Improved dye-sensitized solar cells with a ZnO-nanoflower photoanode. *Appl. Phys. Lett.* **2007**, *90*, 263501. [CrossRef]
15. Wang, C.X.; Yin, L.W.; Zhang, L.Y.; Xiang, D.; Gao, R. Metal oxide gas sensors: Sensitivity and influencing factors. *Sensors* **2010**, *10*, 2088–2106. [CrossRef] [PubMed]
16. Wang, Z.L.; Song, J.H. Piezoelectric nanogenerators based on zinc oxide nanowire arrays. *Science* **2006**, *312*, 242–246. [CrossRef] [PubMed]
17. Ozgur, U.; Alivov, Y.I.; Liu, C.; Teke, A.; Reshchikov, M.A.; Dogan, S.; Avrutin, V.; Cho, S.J.; Morkoc, H. A comprehensive review of ZnO materials and devices. *J. Appl. Phys.* **2005**, *98*, 041301. [CrossRef]
18. Fu, Y.Q.; Luo, J.K.; Du, X.Y.; Flewitt, A.J.; Li, Y.; Markx, G.H.; Walton, A.J.; Milne, W.I. Recent developments on ZnO films for acoustic wave based bio-sensing and microfluidic applications: A review. *Sens. Actuators B Chem.* **2010**, *143*, 606–619. [CrossRef]
19. Fortunato, E.; Barquinha, P.; Martins, R. Oxide semiconductor thin-film transistors: A review of recent advances. *Adv. Mater.* **2012**, *24*, 2945–2986. [CrossRef] [PubMed]

20. Eranna, G.; Joshi, B.C.; Runthala, D.P.; Gupta, R.P. Oxide materials for development of integrated gas sensors—A comprehensive review. *Crit. Rev. Solid State Mater. Sci.* **2004**, *29*, 111–188. [CrossRef]
21. Tanev, P.T.; Pinnavaia, T.J. Mesoporous silica molecular sieves prepared by ionic and neutral surfactant templating: A comparison of physical properties. *Chem. Mater.* **1996**, *8*, 2068–2079. [CrossRef]
22. Romero-Gomez, P.; Toudert, J.; Sanchez-Valencia, J.R.; Borras, A.; Barranco, A.; Gonzalez-Elipe, A.R. Tunable nanostructure and photoluminescence of columnar ZnO films grown by plasma deposition. *J. Phys. Chem. C* **2010**, *114*, 20932–20940. [CrossRef]
23. Sanchez-Valencia, J.R.; Alcaire, M.; Romero-Gomez, P.; Macias-Montero, M.; Aparicio, F.J.; Borras, A.; Gonzalez-Elipe, A.R.; Barranco, A. Oxygen optical sensing in gas and liquids with nanostructured ZnO thin films based on exciton emission detection. *J. Phys. Chem. C* **2014**, *118*, 9852–9859. [CrossRef]
24. Ramos, F.J.; Lopez-Santos, M.C.; Guillen, E.; Nazeeruddin, M.K.; Gratzel, M.; Gonzalez-Elipe, A.R.; Ahmad, S. Perovskite solar cells based on nanocolumnar plasma–deposited ZnO thin films. *Chemphyschem* **2014**, *15*, 1148–1153. [CrossRef] [PubMed]
25. Simon, Q.; Barreca, D.; Gasparotto, A.; Maccato, C.; Montini, T.; Gombac, V.; Fornasiero, P.; Lebedev, O.I.; Turner, S.; Van Tendeloo, G. Vertically oriented CuO/ZnO nanorod arrays: From plasma-assisted synthesis to photocatalytic H-2 production. *J. Mater. Chem.* **2012**, *22*, 11739–11747. [CrossRef]
26. Bakrudeen, H.B.; Tsibouklis, J.; Reddy, B.S.R. Facile fabrication of mesoporous ZnO nanospheres for the controlled delivery of captopril. *J. Nanoparticle Res.* **2013**, *15*, 1505. [CrossRef]
27. Zeng, H.B.; Cai, W.P.; Liu, P.S.; Xu, X.X.; Zhou, H.J.; Klingshirn, C.; Kalt, H. ZnO-based hollow nanoparticles by selective etching: Elimination and reconstruction of metal-semiconductor interface, improvement of blue emission and photocatalysis. *ACS Nano* **2008**, *2*, 1661–1670. [CrossRef] [PubMed]
28. Cai, X.L.; Luo, Y.N.; Zhang, W.Y.; Du, D.; Lin, Y.H. pH-sensitive ZnO quantum dots-doxorubicin nanoparticles for lung cancer targeted drug delivery. *ACS Appl. Mater. Inter.* **2016**, *8*, 22442–22450. [CrossRef] [PubMed]
29. Park, W.I.; Yi, G.C.; Kim, M.; Pennycook, S.J. Quantum confinement observed in ZnO/ZnMgO nanorod heterostructures. *Adv. Mater.* **2003**, *15*, 526–529. [CrossRef]
30. Wang, Z.L. Splendid one-dimensional nanostructures of zinc oxide: A new nanomaterial family for nanotechnology. *ACS Nano* **2008**, *2*, 1987–1992. [CrossRef] [PubMed]
31. Yin, M.; Gu, Y.; Kuskovsky, I.L.; Andelman, T.; Zhu, Y.; Neumark, G.F.; O'Brien, S. Zinc oxide quantum rods. *J. Am. Chem. Soc.* **2004**, *126*, 6206–6207. [CrossRef] [PubMed]
32. Singh, S.P.; Arya, S.K.; Pandey, P.; Malhotra, B.D.; Saha, S.; Sreenivas, K.; Gupta, V. Cholesterol biosensor based on rf sputtered zinc oxide nanoporous thin film. *Appl. Phys. Lett.* **2007**, *91*, 063901. [CrossRef]
33. Lai, Y.F.; Huang, J.H.; Chen, Y.C.; Liu, C.P.; Yang, Y.W. Growth of large-area non-polar ZnO film without constraint to substrate using oblique-angle sputtering deposition. *J. Eur. Ceram. Soc.* **2013**, *33*, 1809–1814. [CrossRef]
34. Sharma, P.; Mansingh, A.; Sreenivas, K. Ultraviolet photoresponse of porous ZnO thin films prepared by unbalanced magnetron sputtering. *Appl. Phys. Lett.* **2002**, *80*, 553–555. [CrossRef]
35. Li, L.; Gao, W.; Reeves, R.J. Zinc oxide films by thermal oxidation of zinc thin films. *Surf. Coat. Technol.* **2005**, *198*, 319–323. [CrossRef]
36. Gazia, R.; Chiodoni, A.; Bianco, S.; Lamberti, A.; Quaglio, M.; Sacco, A.; Tresso, E.; Mandracci, P.; Pirri, C.F. An easy method for the room-temperature growth of spongelike nanostructured Zn films as initial step for the fabrication of nanostructured ZnO. *Thin Solid Films* **2012**, *524*, 107–112. [CrossRef]
37. Lamberti, A.; Sacco, A.; Laurenti, M.; Fontana, M.; Pirri, C.F.; Bianco, S. Sponge-like ZnO nanostructures by low temperature water vapor-oxidation method as dye-sensitized solar cell photoanodes. *J. Alloy Comp.* **2014**, *615*, S487–S490. [CrossRef]
38. Lamberti, A.; Gazia, R.; Sacco, A.; Bianco, S.; Quaglio, M.; Chiodoni, A.; Tresso, E.; Pirri, C.F. Coral-shaped ZnO nanostructures for dye-sensitized solar cell photoanodes. *Prog. Photovolt.* **2014**, *22*, 189–197. [CrossRef]
39. Garino, N.; Lamberti, A.; Gazia, R.; Chiodoni, A.; Gerbaldi, C. Cycling behaviour of sponge-like nanostructured ZnO as thin-film Li-ion battery anodes. *J. Alloy Comp.* **2014**, *615*, S454–S458. [CrossRef]
40. Gazia, R.; Motto, P.; Stassi, S.; Sacco, A.; Virga, A.; Lamberti, A.; Canavese, G. Photodetection and piezoelectric response from hard and flexible sponge-like ZnO-based structures. *Nano Energy* **2013**, *2*, 1294–1302. [CrossRef]

41. Gazia, R.; Canavese, G.; Chiodoni, A.; Lamberti, A.; Stassi, S.; Sacco, A.; Bianco, S.; Virga, A.; Tresso, E.; Pirri, C.F. Novel spongelike nanostructured ZnO films: Properties and applications. *J. Alloy Comp.* **2014**, *586*, S331–S335. [CrossRef]
42. Laurenti, M.; Canavese, G.; Stassi, S.; Fontana, M.; Castellino, M.; Pirri, C.F.; Cauda, V. A porous nanobranched structure: An effective way to improve piezoelectricity in sputtered ZnO thin films. *RSC Adv.* **2016**, *6*, 76996. [CrossRef]
43. Laurenti, M.; Canavese, G.; Sacco, A.; Fontana, M.; Bejtka, K.; Castellino, M.; Pirri, C.F.; Cauda, V. Nanobranched ZnO structure: p-type doping induces piezoelectric voltage generation and ferroelectric-photovoltaic effect. *Adv. Mater.* **2015**, *27*, 4218–4223. [CrossRef] [PubMed]
44. Ghosh, P.; Sharma, A.K. Highly *c*-axis oriented growth and optical characterization of ZnO pore-like structures surrounded by craters via pulsed laser deposition. *Silicon* **2017**, *5*, 1–6. [CrossRef]
45. Hartanto, A.B.; Ning, X.; Nakata, Y.; Okada, T. Growth mechanism of ZnO nanorods from nanoparticles formed in a laser ablation plume. *Appl. Phys. A* **2004**, *78*, 299–301. [CrossRef]
46. Sun, Y.W.; Gospodyn, J.; Kursa, P.; Sit, J.; DeCorby, R.G.; Tsui, Y.Y. Dense and porous ZnO thin films produced by pulsed laser deposition. *Appl. Surf. Sci.* **2005**, *248*, 392–396. [CrossRef]
47. Vinodkumar, R.; Navas, I.; Porsezian, K.; Ganesan, V.; Unnikrishnan, N.V.; Pillai, V.P.M. Structural, spectroscopic and electrical studies of nanostructured porous ZnO thin films prepared by pulsed laser deposition. *Spectrochim. Acta A* **2014**, *118*, 724–732. [CrossRef] [PubMed]
48. Ghosh, P.; Sharma, A.K. Pulsed laser deposition and characterization of ZnO nanopores. *Appl. Phys. A* **2016**, *122*, 357. [CrossRef]
49. Sun, Y.W.; Tsui, Y.Y. Production of porous nanostructured zinc oxide thin films by pulsed laser deposition. *Opt. Mater.* **2007**, *29*, 1111–1114. [CrossRef]
50. Wolcott, A.; Smith, W.A.; Kuykendall, T.R.; Zhao, Y.P.; Zhang, J.Z. Photoelectrochemical study of nanostructured ZnO thin films for hydrogen generation from water splitting. *Adv. Funct. Mater.* **2009**, *19*, 1849–1856. [CrossRef]
51. Labis, J.P.; Hezam, M.; Al-Anazi, A.; Al-Brithen, H.; Ansari, A.A.; El-Toni, A.M.; Enriquez, R.; Jacopin, G.; Al-Hoshan, M. Pulsed laser deposition growth of 3D ZnO nanowall network in nest-like structures by two-step approach. *Sol. Energy Mater. Sol. Cells* **2015**, *143*, 539–545. [CrossRef]
52. El Zein, B.; Boulfrad, S.; Jabbour, G.E.; Dogheche, E. Parametric study of self-forming ZnO nanowall network with honeycomb structure by pulsed laser deposition. *Appl. Surf. Sci.* **2014**, *292*, 598–607. [CrossRef]
53. Han, B.S.; Caliskan, S.; Sohn, W.; Kim, M.; Lee, J.K.; Jang, H.W. Room temperature deposition of crystalline nanoporous ZnO nanostructures for direct use as flexible DSSC photoanode. *Nanoscale Res. Lett.* **2016**, *11*, 221. [CrossRef] [PubMed]
54. Achkar, A.; Jedrzejowski, P.; Pignolet, A.; Sarkissian, A. Porous and dense ZnO films produced by femtosecond and picosecond pulsed laser deposition. *J. Optoelectron. Adv. Mater.* **2010**, *12*, 646–649.
55. Dhamodharan, P.; Manoharan, C.; Dhanapandian, S.; Venkatachalam, P. Dye-sensitized solar cell using sprayed ZnO nanocrystalline thin films on ITO as photoanode. *Spectrochim. Acta A* **2015**, *136*, 1671–1678. [CrossRef] [PubMed]
56. Studenikin, S.A.; Golego, N.; Cocivera, M. Fabrication of green and orange photoluminescent, undoped ZnO films using spray pyrolysis. *J. Appl. Phys.* **1998**, *84*, 2287–2294. [CrossRef]
57. Dobrozhan, O.; Kurbatov, D.; Opanasyuk, A.; Cheong, H.; Cabot, A. Influence of substrate temperature on the structural and optical properties of crystalline ZnO films obtained by pulsed spray pyrolysis. *Surf. Interface Anal.* **2015**, *47*, 601–606. [CrossRef]
58. Zahedi, F.; Dariani, R.S.; Rozati, S.M. Structural, optical and electrical properties of ZnO thin films prepared by spray pyrolysis: Effect of precursor concentration. *Bull. Mater. Sci.* **2014**, *37*, 433–439. [CrossRef]
59. Benramache, S.; Rahal, A.; Benhaoua, B. The effects of solvent nature on spray-deposited ZnO thin film prepared from $Zn(CH_3COO)_2$, $2H_2O$. *Optik* **2014**, *125*, 663–666. [CrossRef]
60. Mani, G.K.; Rayappan, J.B.B. Impact of annealing duration on spray pyrolysis deposited nanostructured zinc oxide thin films. *Superlattice Microstruct.* **2014**, *67*, 82–87. [CrossRef]
61. Shaban, Z.; Ara, M.H.M.; Falahatdoost, S.; Ghazyani, N. Optimization of ZnO thin film through spray pyrolysis technique and its application as a blocking layer to improving dye sensitized solar cell efficiency. *Curr. Appl. Phys.* **2016**, *16*, 131–134. [CrossRef]

62. Mani, G.K.; Rayappan, J.B.B. Novel and facile synthesis of randomly interconnected ZnO nanoplatelets using spray pyrolysis and their room temperature sensing characteristics. *Sens. Actuators B Chem.* **2014**, *198*, 125–133. [CrossRef]
63. Mani, G.K.; Rayappan, J.B.B. A highly selective room temperature ammonia sensor using spray deposited zinc oxide thin film. *Sens. Actuators B Chem.* **2013**, *183*, 459–466. [CrossRef]
64. Mariappan, R.; Ponnuswamy, V.; Suresh, P.; Ashok, N.; Jayamurugan, P.; Bose, A.C. Influence of film thickness on the properties of sprayed ZnO thin films for gas sensor applications. *Superlattice Microstruct.* **2014**, *71*, 238–249. [CrossRef]
65. Shewale, P.S.; Agawane, G.L.; Shin, S.W.; Moholkar, A.V.; Lee, J.Y.; Kim, J.H.; Uplane, M.D. Thickness dependent H_2S sensing properties of nanocrystalline ZnO thin films derived by advanced spray pyrolysis. *Sens. Actuators B Chem.* **2013**, *177*, 695–702. [CrossRef]
66. Tarwal, N.L.; Rajgure, A.V.; Inamdar, A.I.; Devan, R.S.; Kim, I.Y.; Suryavanshi, S.S.; Ma, Y.R.; Kim, J.H.; Patil, P.S. Growth of multifunctional ZnO thin films by spray pyrolysis technique. *Sens. Actuators A Phys.* **2013**, *199*, 67–73. [CrossRef]
67. Ammaih, Y.; Lfakir, A.; Hartiti, B.; Ridah, A.; Thevenin, P.; Siadat, M. Structural, optical and electrical properties of ZnO:Al thin films for optoelectronic applications. *Opt. Quant. Electron.* **2014**, *46*, 229–234. [CrossRef]
68. Mahadik, M.A.; Hunge, Y.M.; Shinde, S.S.; Rajpure, K.Y.; Bhosale, C.H. Semiconducting properties of aluminum-doped ZnO thin films grown by spray pyrolysis technique. *J. Semicond.* **2015**, *36*, 033002. [CrossRef]
69. Allah, F.K.; Abe, S.Y.; Nunez, C.M.; Khelil, A.; Cattin, L.; Morsli, M.; Bernede, J.C.; Bougrine, A.; del Valle, M.A.; Diaz, F.R. Characterisation of porous doped ZnO thin films deposited by spray pyrolysis technique. *Appl. Surf. Sci.* **2007**, *253*, 9241–9247. [CrossRef]
70. Hameed, M.S.; Princice, J.J.; Babu, N.R.; Arunachalam, A. Effect of silver doping on optical properties of nanoflower ZnO thin films prepared by spray pyrolysis technique. *J. Mater. Sci. Mater. Electron.* **2017**, *28*, 8675–8683. [CrossRef]
71. Mariappan, R.; Ponnuswamy, V.; Suresh, R.; Suresh, P.; Bose, A.C.; Ragavendar, M. Role of substrate temperature on the properties of Na-doped ZnO thin film nanorods and performance of ammonia gas sensors using nebulizer spray pyrolysis technique. *J. Alloy Comp.* **2014**, *582*, 387–391. [CrossRef]
72. Kurtaran, S.; Aldag, S.; Ofofoglu, G.; Akyuz, I.; Atay, F. Transparent conductive ZnO thin films grown by chemical spray pyrolysis: The effect of Mg. *J. Mater. Sci. Mater. Electron.* **2016**, *27*, 8478–8485. [CrossRef]
73. Dhasmana, H.; Shital, S.; Dutta, V. ZnO nanostructure thin films by continuous spray pyrolysis using doped precursor for Si solar cell application. *J. Mater. Sci. Mater. Electron.* **2014**, *25*, 4095–4102. [CrossRef]
74. Shewale, P.S.; Yu, Y.S. H_2S gas sensing properties of undoped and Ti doped ZnO thin films deposited by chemical spray pyrolysis. *J. Alloy Comp.* **2016**, *684*, 428–437. [CrossRef]
75. Mani, G.K.; Rayappan, J.B.B. Facile synthesis of ZnO nanostructures by spray pyrolysis technique and its application as highly selective H_2S sensor. *Mater. Lett.* **2015**, *158*, 373–376. [CrossRef]
76. Shewale, P.S.; Patil, V.B.; Shin, S.W.; Kim, J.H.; Uplane, M.D. H_2S gas sensing properties of nanocrystalline Cu-doped ZnO thin films prepared by advanced spray pyrolysis. *Sens. Actuators B Chem.* **2013**, *186*, 226–234. [CrossRef]
77. Mani, G.K.; Rayappan, J.B.B. Selective detection of ammonia using spray pyrolysis deposited pure and nickel doped ZnO thin films. *Appl. Surf. Sci.* **2014**, *311*, 405–412. [CrossRef]
78. Muniyandi, I.; Mani, G.K.; Shankar, P.; Rayappan, J.B.B. Effect of nickel doping on structural, optical, electrical and ethanol sensing properties of spray deposited nanostructured ZnO thin films. *Ceram. Int.* **2014**, *40*, 7993–8001. [CrossRef]
79. Zhang, X.M.; Dong, Z.J.; Liu, S.; Yan, S.; Dong, Y.H.; Wei, F. Maize straw-templated hierarchical porous ZnO:Ni with enhanced acetone gas sensing properties. *Sens. Actuators B Chem.* **2017**, *243*, 1224–1230. [CrossRef]
80. El khalidi, Z.; Comini, E.; Hartiti, B.; Moumen, A.; Munasinghe Arachchige, H.M.M.; Fadili, S.; Thevenin, P.; Kamal, A. Effect of vanadium doping on ZnO sensing properties synthesized by spray pyrolysis. *Mater. Des.* **2018**, *139*, 56–64. [CrossRef]
81. Kulandaisamy, A.J.; Reddy, J.R.; Srinivasan, P.; Babu, K.J.; Mani, G.K.; Shankar, P.; Rayappan, J.B.B. Room temperature ammonia sensing properties of ZnO thin films grown by spray pyrolysis: Effect of Mg doping. *J. Alloy Comp.* **2016**, *688*, 422–429. [CrossRef]

82. Duta, M.; Perniu, D.; Duta, A. Photocatalytic zinc oxide thin films obtained by surfactant assisted spray pyrolysis deposition. *Appl. Surf. Sci.* **2014**, *306*, 80–88. [CrossRef]
83. Ravichandran, K.; Mohan, R.; Sakthivel, B.; Varadharajaperumal, S.; Devendran, P.; Alagesan, T.; Pandian, K. Enhancing the photocatalytic efficiency of sprayed ZnO thin films through double doping (Sn plus F) and annealing under different ambiences. *Appl. Surf. Sci.* **2014**, *321*, 310–317. [CrossRef]
84. Dhamodharan, P.; Manoharan, C.; Dhanapandian, S.; Bououdina, M.; Ramalingam, S. Preparation and characterization of spray deposited Sn-doped ZnO thin films onto ITO subtracts as photoanode in dye sensitized solar cell. *J. Mater. Sci. Mater. Electron.* **2015**, *26*, 4830–4839. [CrossRef]
85. Manoharan, C.; Pavithra, G.; Dhanapandian, S.; Dhamodharan, P. Effect of in doping on the properties and antibacterial activity of ZnO films prepared by spray pyrolysis. *Spectrochim. Acta A* **2015**, *149*, 793–799. [CrossRef] [PubMed]
86. Vasanthi, M.; Ravichandran, K.; Begum, N.J.; Muruganantham, G.; Snega, S.; Panneerselvam, A.; Kavitha, P. Influence of Sn doping level on antibacterial activity and certain physical properties of ZnO films deposited using a simplified spray pyrolysis technique. *Superlattice Microstruct.* **2013**, *55*, 180–190. [CrossRef]
87. Michaelis, E.; Wohrle, D.; Rathousky, J.; Wark, M. Electrodeposition of porous zinc oxide electrodes in the presence of sodium laurylsulfate. *Thin Solid Films* **2006**, *497*, 163–169. [CrossRef]
88. Kim, Y.K.; Hwang, S.H.; Kim, S.; Park, H.; Lim, S.K. ZnO nanostructure electrodeposited on flexible conductive fabric: A flexible photo-sensor. *Sens. Actuators B Chem.* **2017**, *240*, 1106–1113. [CrossRef]
89. Lv, J.G.; Wang, W.H.; Zhao, M.; Zhu, W.L.; Cheng, Y.B.; He, G.; Zhang, M.; Chen, X.S.; Sun, Z.Q. Enhanced visible light response of ZnO porous thin film by post-annealing treatment. *J. Mater. Sci. Mater. Electron.* **2017**, *28*, 4051–4057. [CrossRef]
90. Reemts, J.; Kittel, A. Persistent photoconductivity in highly porous ZnO films. *J. Appl. Phys.* **2007**, *101*, 013709. [CrossRef]
91. Chen, Z.G.; Tang, Y.W.; Zhang, L.S.; Luo, L.J. Electrodeposited nanoporous ZnO films exhibiting enhanced performance in dye-sensitized solar cells. *Electrochim. Acta* **2006**, *51*, 5870–5875. [CrossRef]
92. Venditti, L.; Barbero, N.; Russo, M.V.; Di Carlo, A.; Decker, F.; Fratoddi, I.; Barolo, C.; Dini, D. Electrodeposited ZnO with squaraine sentisizers as photoactive anode of DSCs. *Mater. Res. Express* **2014**, *1*, 015040. [CrossRef]
93. Dunkel, C.; Wark, M.; Oekermann, T.; Ostermann, R.; Smarsly, B.M. Electrodeposition of zinc oxide on transparent conducting metal oxide nanofibers and its performance in dye sensitized solar cells. *Electrochim. Acta* **2013**, *90*, 375–381. [CrossRef]
94. Pauporte, T.; Rathousky, J. Electrodeposited mesoporous ZnO thin films as efficient photocatalysts for the degradation of dye pollutants. *J. Phys. Chem. C* **2007**, *111*, 7639–7644. [CrossRef]
95. Dikici, T. Temperature-dependent growth of ZnO structures by thermal oxidation of Zn coatings electrodeposited on steel substrates and their photocatalytic activities. *Ceram. Int.* **2017**, *43*, 8289–8293. [CrossRef]
96. Wanotayan, T.; Panpranot, J.; Qin, J.; Boonyongmaneerat, Y. Microstructures and photocatalytic properties of ZnO films fabricated by Zn electrodeposition and heat treatment. *Mater. Sci. Semicond. Proc.* **2018**, *74*, 232–237. [CrossRef]
97. Lu, H.; Zhang, M.; Guo, M. Controllable electrodeposition of ZnO nanorod arrays on flexible stainless steel mesh substrate for photocatalytic degradation of Rhodamine B. *Appl. Surf. Sci.* **2014**, *317*, 672–681. [CrossRef]
98. Yang, J.; Wang, Y.Q.; Kong, J.H.; Jia, H.X.; Wang, Z.S. Synthesis of ZnO nanosheets via electrodeposition method and their optical properties, growth mechanism. *Opt. Mater.* **2015**, *46*, 179–185. [CrossRef]
99. Li, H.; Yu, S.R.; Han, X.X. Preparation of a biomimetic superhydrophobic ZnO coating on an X90 pipeline steel surface. *New J. Chem.* **2015**, *39*, 4860–4868.
100. Li, M.; Zhai, J.; Liu, H.; Song, Y.L.; Jiang, L.; Zhu, D.B. Electrochemical deposition of conductive superhydrophobic zinc oxide thin films. *J. Phys. Chem. B* **2003**, *107*, 9954–9957. [CrossRef]
101. Pal, B.; Sharon, M. Enhanced photocatalytic activity of highly porous ZnO thin films prepared by sol-gel process. *Mater. Chem. Phys.* **2002**, *76*, 82–87. [CrossRef]
102. Wang, C.F.; Tzeng, F.S.; Chen, H.G.; Chang, C.J. Ultraviolet-durable superhydrophobic zinc oxide-coated mesh films for surface and underwater-oil capture and transportation. *Langmuir* **2012**, *28*, 10015–10019. [CrossRef] [PubMed]
103. Zhang, J.; Wang, S.R.; Xu, M.J.; Wang, Y.; Zhu, B.L.; Zhang, S.M.; Huang, W.P.; Wu, S.H. Hierarchically porous ZnO architectures for gas sensor application. *Cryst. Growth Des.* **2009**, *9*, 3532–3537. [CrossRef]

104. Chatterjee, A.P.; Mitra, P.; Mukhopadhyay, A.K. Chemically deposited zinc oxide thin film gas sensor. *J. Mater. Sci.* **1999**, *34*, 4225–4231. [CrossRef]
105. Hosono, E.; Fujihara, S.; Kimura, T.; Imai, H. Growth of layered basic zinc acetate in methanolic solutions and its pyrolytic transformation into porous zinc oxide films. *J. Colloid Interface Sci.* **2004**, *272*, 391–398. [CrossRef] [PubMed]
106. Wang, H.H.; Xie, C.S. Controlled fabrication of nanostructured ZnO particles and porous thin films via a modified chemical bath deposition method. *J. Cryst. Growth* **2006**, *291*, 187–195. [CrossRef]
107. Wang, H.H.; Dong, S.J.; Chang, Y.; Zhou, X.P.; Hu, X.B. Microstructures and photocatalytic properties of porous ZnO films synthesized by chemical bath deposition method. *Appl. Surf. Sci.* **2012**, *258*, 4288–4293. [CrossRef]
108. Ottone, C.; Bejtka, K.; Chiodoni, A.; Farias, V.; Roppolo, I.; Canavese, G.; Stassi, S.; Cauda, V. Comprehensive study of the templating effect on the ZnO nanostructure formation within porous hard membranes. *New J. Chem.* **2014**, *38*, 2058–2065. [CrossRef]
109. Ottone, C.; Rivera, V.F.; Fontana, M.; Bejtka, K.; Onida, B.; Cauda, V. Ultralong and mesoporous ZnO and gamma-Al_2O_3 oriented nanowires obtained by template-assisted hydrothermal approach. *J. Mater. Sci. Technol.* **2014**, *30*, 1167–1173. [CrossRef]
110. Ryu, H.W.; Park, B.S.; Akbar, S.A.; Lee, W.S.; Hong, K.J.; Seo, Y.J.; Shin, D.C.; Park, J.S.; Choi, G.P. ZnO sol-gel derived porous film for CO gas sensing. *Sens. Actuators B Chem.* **2003**, *96*, 717–722. [CrossRef]
111. Leone, F.; Gignone, A.; Ronchetti, S.; Cavalli, R.; Manna, L.; Banchero, M.; Onida, B. A green organic-solvent-free route to prepare nanostructured zinc oxide carriers of clotrimazole for pharmaceutical applications. *J. Clean. Prod.* **2018**, *172*, 1433–1439. [CrossRef]
112. Liu, Z.F.; Jin, Z.G.; Li, W.; Qiu, J.J.; Zhao, J.; Liu, X.X. Synthesis of PS colloidal crystal templates and ordered ZnO porous thin films by dip-drawing method. *Appl. Surf. Sci.* **2006**, *252*, 5002–5009. [CrossRef]
113. Yan, H.W.; Yang, Y.L.; Fu, Z.P.; Yang, B.F.; Xia, L.S.; Fu, S.Q.; Li, F.Q. Fabrication of 2D and 3D ordered porous ZnO films using 3D opal templates by electrodeposition. *Electrochem. Commun.* **2005**, *7*, 1117–1121. [CrossRef]
114. Liu, Z.F.; Jin, Z.G.; Li, W.; Qiu, J.J. Preparation of ZnO porous thin films by sol-gel method using PEG template. *Mater. Lett.* **2005**, *59*, 3620–3625. [CrossRef]
115. Liu, Z.F.; Jin, Z.G.; Qiu, J.J.; Liu, X.X.; Wu, W.B.; Li, W. Preparation and characteristics of ordered porous ZnO films by a electrodeposition method using PS array templates. *Semicond. Sci. Technol.* **2006**, *21*, 60–66. [CrossRef]
116. Liu, Z.F.; Jin, Z.G.; Li, W.; Liu, X.X. Ordered porous ZnO thin films formed by dip-coating method using PS templates. *J. Sol-Gel Sci. Technol.* **2006**, *40*, 25–30. [CrossRef]
117. Cao, B.Q.; Cai, W.P.; Sun, F.Q.; Li, Y.; Lei, Y.; Zhang, L.D. Fabrication of large-scale zinc oxide ordered pore arrays with controllable morphology. *Chem. Commun.* **2004**, 1604–1605. [CrossRef] [PubMed]
118. Eltayeb, A.; Daniels, S.; McGlynn, E. Enhanced optical properties of ZnO and CeO_2-coated ZnO nanostructures achieved via spherical nanoshells growth on a polystyrene template. *Sci. Rep.* **2017**, *7*, 3737. [CrossRef] [PubMed]
119. Xiong, Y.Y.; Kang, F.; Ke, Z.; Zhuo, S.Y.; Liang, C.F.; Zhang, Z.X. Fabrication and characterization of three-dimensional core-shell structure ZnO photonic crystals by magnetron sputtering based on opal template. *J. Cryst. Growth* **2010**, *312*, 2484–2488.
120. Lin, X.; Chen, M. Fabrication and photo-detecting performance of 2D ZnO inverse opal films. *Appl. Sci.* **2016**, *6*, 259. [CrossRef]
121. Wang, Z.H.; Tian, Z.W.; Han, D.M.; Gu, F.B. Highly sensitive and selective ethanol sensor fabricated with In-doped 3DOM ZnO. *ACS Appl. Mater. Inter.* **2016**, *8*, 5466–5474. [CrossRef] [PubMed]
122. Su, X.S.; Duan, G.T.; Xu, Z.K.; Zhou, F.; Cai, W.P. Structure and thickness-dependent gas sensing responses to NO_2 under UV irradiation for the multilayered ZnO micro/nanostructured porous thin films. *J. Colloid Interface Sci.* **2017**, *503*, 150–158. [CrossRef] [PubMed]
123. Cheng, K.; Li, Q.Q.; Meng, J.; Han, X.; Wu, Y.Q.; Wang, S.J.; Qian, L.; Du, Z.L. Interface engineering for efficient charge collection in Cu_2O/ZnO heterojunction solar cells with ordered ZnO cavity-like nanopatterns. *Sol. Energy Mater. Sol. Cells* **2013**, *116*, 120–125. [CrossRef]
124. Kim, E.; Vaynzof, Y.; Sepe, A.; Guldin, S.; Scherer, M.; Cunha, P.; Roth, S.V.; Steiner, U. Gyroid-structured 3D ZnO networks made by atomic layer deposition. *Adv. Funct. Mater.* **2014**, *24*, 863–872. [CrossRef]

125. Yong, J.L.; Chen, F.; Yang, Q.; Fang, Y.; Huo, J.L.; Hou, X. Femtosecond laser induced hierarchical ZnO superhydrophobic surfaces with switchable wettability. *Chem. Commun.* **2015**, *51*, 9813–9816. [CrossRef] [PubMed]
126. Balela, M.D.L.; Pelicano, C.M.O.; Ty, J.D.; Yanagi, H. Formation of zinc oxide nanostructures by wet oxidation of vacuum deposited Zn thin film. *Opt. Quant. Electron.* **2017**, *49*, 3. [CrossRef]
127. Alcaire, M.; Filippin, A.N.; Macias-Montero, M.; Sanchez-Valencia, J.R.; Rojas, T.C.; Mora-Boza, A.; Lopez-Santos, C.; Espinos, J.P.; Barranco, A.; Borras, A. Highly porous ZnO thin films and 1D nanostructures by remote plasma processing of Zn-phthalocyanine. *Plasma. Process. Polym.* **2016**, *13*, 287–297. [CrossRef]
128. Wang, H.J.; Sun, Y.Y.; Cao, Y.; Yu, X.H.; Ji, X.M.; Yang, L. Porous zinc oxide films: Controlled synthesis, cytotoxicity and photocatalytic activity. *Chem. Eng. J.* **2011**, *178*, 8–14. [CrossRef]
129. Sacco, A.; Lamberti, A.; Gazia, R.; Bianco, S.; Manfredi, D.; Shahzad, N.; Cappelluti, F.; Ma, S.; Tresso, E. High efficiency dye-sensitized solar cells exploiting sponge-like ZnO nanostructures. *Phys. Chem. Chem. Phys.* **2012**, *14*, 16203–16208. [CrossRef] [PubMed]

© 2018 by the authors. Licensee MDPI, Basel, Switzerland. This article is an open access article distributed under the terms and conditions of the Creative Commons Attribution (CC BY) license (http://creativecommons.org/licenses/by/4.0/).